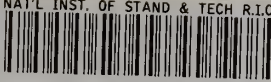


A11100 156864

NBS  
PUBLICATIONS

NAT'L INST. OF STAND & TECH R.I.C.



A11105 156864

**NBSIR 80-2058 (ONR)**

# **Studies of Microscopic Aspects of Wear Processes in Metals**

---

A. W. Ruff  
P. J. Blau

Metallurgy Division  
Center for Materials Science  
National Measurement Laboratory  
National Bureau of Standards  
U.S. Department of Commerce  
Washington, DC 20234

April 1, 1979-December 31, 1979  
Annual Report  
N00014-79-F-0034  
NR 091-011/2-14-79(473)  
Issued June 1980

QC ~~\_\_\_\_\_~~ for:  
 100 of Naval Research  
 U56 ent of the Navy  
 80-2058 n, VA 22217  
 1980  
 c.2



SEP 19 1980

not acc - line

20100

11381

85-3052

1980

0.5

NBSIR 80-2058 (ONR)

**STUDIES OF MICROSCOPIC ASPECTS OF  
WEAR PROCESSES IN METALS**

---

A. W. Ruff  
P. J. Blau

Metallurgy Division  
Center for Materials Science  
National Measurement Laboratory  
National Bureau of Standards  
U.S. Department of Commerce  
Washington, DC 20234

April 1, 1979-December 31, 1979  
Annual Report  
N00014-79-F-0034  
NR 091-011/2-14-79(473)

Issued June 1980

Reproduction in whole or in part is permitted for any purpose of the United States Government

Prepared for:  
Office of Naval Research  
Department of the Navy  
Arlington, VA 22217



---

**U.S. DEPARTMENT OF COMMERCE, Philip M. Klutznick, Secretary**

**Luther H. Hodges, Jr., Deputy Secretary**

**Jordan J. Baruch, Assistant Secretary for Productivity, Technology, and Innovation**

**NATIONAL BUREAU OF STANDARDS, Ernest Ambler, Director**

THE UNIVERSITY OF CHICAGO  
DEPARTMENT OF CHEMISTRY

RECEIVED  
MAY 10 1912

BY  
DR. J. H. VAN VORN

PH.D. THESIS



THE UNIVERSITY OF CHICAGO  
DEPARTMENT OF CHEMISTRY  
CHICAGO, ILL.

## Abstract

Wear experiments have been conducted in copper alloys and steels under dry sliding conditions in order to study the microscopic aspects of wear and the mechanisms involved. Two experimental wear test systems have been developed: a linear sliding tester and a block-on-ring computer controlled tester. Preliminary findings have compared the wear rates of three different steels, one a high strength-low alloy "dual phase" steel, and two copper-aluminum alloys. Worn surface and subsurface morphologies have been studied using optical and scanning electron microscopy. Wear debris particles have been recovered from the tests and compared in morphological characteristics between the materials. Mechanical properties measurements of two of the steels were carried out to determine strain hardening characteristics for comparison with wear behavior. Micro-hardness measurements have also been made. Initial wear rate and friction transients for tests in laboratory air and argon have been examined to study processes involved in the early stages of sliding.

## TABLE OF CONTENTS

### Introduction

#### I. Experimental Approach

##### A. Wear Test Systems

1. Block-on-ring system
2. Linear tribometer system

#### II. Materials Considerations

#### III. Results and Discussion

##### A. Wear Experiments

1. Break-in studies
  - (a) Linear tribometer results
  - (b) Block-on-ring results
2. Wear studies
  - (a) Steel alloys
  - (b) Copper alloys

##### B. Mechanical Properties Measurements

#### IV. Summary and Plans

### Acknowledgements

## Introduction

This annual report will describe the findings in a project concerned with microscopic aspects of wear processes in metals. The initial phase of research has been concerned with establishing a wear testing and wear measurement capability, obtaining wear data in two different alloy systems (iron-based and copper-based alloys), and obtaining microscopic evidence on significant wear factors from surface, sub-surface and wear debris studies. Mechanical properties data have also been obtained for examination of materials parameter effects in wear. Plans for continued research into the questions opened here will be described at the conclusion of this report.

The presently inadequate state of quantitative understanding of material wear is due in large measure to the complexity of the subject. Research studies have identified several different wear mechanisms and wear processes that may combine or appear at different times in a practical situation. However, an adequate understanding even of the separate wear mechanisms already identified does not exist in most cases. This is particularly true with regard to material parameter effects on wear. Therefore the prospects for extending the knowledge from simple wearing situations to complex ones are not promising at the present time. In principle such an approach should be possible. It is believed that an improved quantitative understanding of basic wear processes should result from properly designed experimental and theoretical investigations. Emphasis at this time is needed from the viewpoint of metallurgy and materials science, particularly in focusing on the microscopic scale of basic wear interactions as well as on materials properties in the surface and the near-surface regions.

This research project is studying three specific aspects of the wear problem: wear mechanisms, wear debris formation processes and material parameter effects on wear. Attention will be directed to both initial phases and steady-state phases of the wear process. Prior to the onset of a steady-state wear condition (i.e. constant rate of wear), a characteristic behavior in numerous metallic sliding systems occurs known as the run-in, or break-in, period. During this period initial surface finishes, oxide and contaminant effects, and changing geometric loading conditions may produce significant friction and wear transients. The break-in stage establishes the conditions for steady state that follows. Below the metal contact surfaces during break-in, initial microstructures are subjected to directional surface tractions which may result in the formation of highly strained and crystallographically textured zones. The nature of such deformed zones is not well understood. Metallographic studies are underway in this project to examine some of the microstructural evolutionary processes which may affect the tribological response of the system, including friction transients, during the break-in period. The role of the surface and near-surface material in steady state wear is also being examined. Attention here is being directed toward the development of subsurface strains, subsurface microstructure, voids, cracks, etc., below the contact surface as a result of sliding wear. The significance of fatigue and fracture also are being examined in the different phases of wear.

The wear mechanism that operates under a specific set of experimental conditions will lead to wear debris formation as well as the establishment of a particular surface morphology, structure, and deformation substructure in the specimen. The microscopic processes by which debris particles are formed are being studied in this project through a series of controlled



experiments involving changes in materials, environment and loading conditions. Debris particles are being characterized with respect to size, shape and morphology. Those observations when compared with wear surface structures will enable us to develop conclusions regarding the debris formation process involving plastic elongation and ductile failure of surface microfeatures.

This project will also examine the effect on wear of limited changes in certain material parameters, such as fatigue resistance, toughness, ductility, strain hardening coefficient, and environmental sensitivity. It is believed that a proper combination of measurable material parameters can be shown to strongly influence wear rates, at least under certain conditions. One example of a potentially significant material parameter concerns the plastic strain hardening characteristic which can be altered through alloying changes within one crystal system (and also varied among alloys of different crystal structure). Significant changes in the formability of steels are known to result from minor changes in alloying additions and processing conditions. Experiments involving microalloyed steels are being undertaken to indicate whether the microalloying approach to provide improved mechanical properties can also offer wear benefits.

## I. Experimental Approach

### A. *Wear test systems*

#### 1. Block-on-ring system

Two wear test systems were developed for use in this study. One involved a test configuration of conventional block-on-ring geometry utilizing a variable speed 1/4 h.p. electric motor with a replaceable standard wear ring (3.49 cm diameter, 8.7 mm wide) attached to the motor shaft to provide sliding motion for

the wear test (Fig. 1). The test specimen was loaded on top of this ring and was held in place on an instrumented arm which was free to pivot in a vertical plane. The holder used for the rectangular block specimens (0.63x1.27x2.54 cm) was designed so that weights could be placed over the contact in order to vary the load. A load of 10 N was used in all tests with this system. A clear plastic enclosure around the wear contact region was used to maintain a flowing argon atmosphere and a low humidity level during the dry wear tests. A cam surface on the wear ring holder on the motor shaft was used to open and close a switch in a D.C. circuit, once per cycle. This switch was used to synchronize data sampling with the motor shaft position to reduce the contribution to displacement due to the wear ring surface run-out. Surface run-out was typically 10  $\mu\text{m}$ , however, this data sampling method reduced the effect by a factor of 100. Wear debris was collected on a clean glass slide positioned below the wear contact. All the experiments carried out with this system used a sliding speed of 20 cm/s (110 RPM).

The 52100 steel ring and specimen block were fastened in place after cleaning in hexane and acetone. The alloy blocks were previously metallographically polished through 600 grit SiC paper (through 1  $\mu\text{m}$  diamond polishing for the copper alloys). The block specimens were aligned using two set screws in the specimen holder. A small light was used to illuminate the contact area between the block and the ring and a magnifier was used to inspect the contact for parallel surfaces. When the specimen was properly aligned, argon was introduced **into the** chamber for wear tests. After about 5-10 minutes of argon flow the test was begun. When the test was completed the wear debris slide and specimen were removed and the ring was

cleaned with hexane and acetone to remove loose wear debris. Test rings were changed whenever a new type of specimen was tested or when the rings began to show significant wear. Typically two to four tests were conducted on one 52100 steel ring.

The block-on-ring wear test system was interfaced to a mini-computer system for control and data acquisition purposes. Four parameters were measured: contact friction, contact displacement, enclosure or specimen (bulk) temperature, and time, in a repeating cycle. Contact displacement was measured with a linear variable differential transducer (LVDT) which monitored the change in height of the specimen holder relative to the ring surface. Friction was monitored through the use of two strain gauges attached to the pivoting arm; the resulting signal was directed to an amplifier. Temperature was measured by a thermocouple placed within the enclosure or welded to the specimen. Running time was determined by the computer internal clock. The input signals were directed to an addressable switch scanner (100 Hz switching rate) and then to a programmable digital voltmeter (25 Hz reading rate). Program control enables the computer to select a scanner channel, set the range and operating mode for the voltmeter and then read a value from the voltmeter. Data were printed as needed during the wear test; usually the average of 10 readings at a 2 Hz rate. Data were also recorded for processing using the computer and a plotter. Processing software was developed to examine and plot friction vs time, wear displacement vs time, and wear volume vs time. The wear displacement and wear volume plots could be made with either the raw data or with averaged data.

## 2. Linear tribometer system

A schematic representation of the second wear system, a ball-on-flat linear tribometer, is shown in Fig. 2. In the figure, A is the flat specimen being tested (mechanically polished through 1  $\mu\text{m}$  diamond paste), B is a 52100 steel ball bearing (0.635 cm diam.) mounted on a brass stub, C is a drill rod guide pin through a high precision linear ball bushing and D is a 304 stainless steel proving ring containing a strain gauge (not shown) mounted on the outside surface. The arrow shows the movement of Specimen A, relative to the ball, B. The friction head was mounted above the traversing table of a bench-top milling machine. The sliding velocity was 0.45 cm/s in all tests and the loads on the ball were 250 g and 500 g (2.45 N and 4.91 N). Loading weights were placed directly above the ball on the protruding end of the ball mounting stub. Prior to testing, each specimen and ball surface was cleaned in hexane, acetone, and methanol. Tests were conducted in laboratory air environments. An enclosure is being constructed for future tests in argon gas. A "dummy" rider stub containing a pulley-mounted wire was substituted for the rider ball in order to calibrate friction force. Weights were applied to give a horizontal deflection of the proving ring. The strain gauge output was fed to a strain gauge conditioner, and then to the Y drive of an X-Y recorder. Calibration was performed before and after each track was worn. The recorder X axis was set at a constant time-base scan rate so that it represented the position of the ball rider along the wear track (at constant sliding velocity). In this way frictional force (hence, friction coefficient) was plotted as a function of position along the track. Multi-pass experiments were performed in a unidirectional sliding mode with the rider manually reset between subsequent passes.

## B. *Mechanical Testing*

Tensile deformation characteristics of two of the steels studied here were carried out using a commercial screw-type tensile machine. Tests were conducted at a cross head extension rate of 0.5 mm/min at room temperature. The yield stress was determined at 0.2% plastic elongation, and the tensile strength at fracture. The reduction-in-area was determined using traveling microscope measurements of the initial and final cross-section of each specimen. The tensile specimens were machined by milling from the 1015 steel material and the dual phase steel. Prior to testing the specimens were lightly polished to remove residual machining marks from the 2.5 cm gauge length. True stress-true strain data were obtained from each test and will be described later.

## II. Materials Considerations

Two alloy systems are being studied in this project. Iron-based alloys of three types are included at present: a plain carbon steel, a type of microalloyed (dual phase) steel and a tool steel. Pure copper and copper-based alloys containing aluminum as a solute are also under investigation. These two alloy systems are in extensive use in tribological applications; therefore, improved wear data and an increased understanding of the mechanisms involved should have a demonstrable impact on applications.

Plain carbon steels are utilized in many wearing situations, involving both dry and lubricated environments, since they offer a low cost materials option. For simplicity and purposes of comparison, a low carbon AISI 1015 type steel has been selected for study here. The composition was 0.14% C, 0.4% Mn, 0.04% P, 0.05% S, the balance being iron. The material was obtained in strip form, 3.2 mm thick and 19 mm wide. Specimens for wear testing and for tensile testing were machined from this strip and

normalized at 925°C in evacuated glass vials prior to testing. The microstructure prior to wear testing is shown in Fig. 3a.

Microalloyed high-strength steels are currently available [1]\* with a broad range of characteristics for many structural applications including buildings, bridges, pilings and pressure vessels. Yield strengths in the as-hot-rolled condition range up to about 550 MPa, about twice that of conventional mild steels that are customarily used for structural purposes. The so-called high strength, low alloy (HSLA) or microalloyed steels contain small amounts of alloy elements such as copper, chromium, columbium, silicon, vanadium and others, and a relatively low carbon content of about 0.2%. Strengthening is achieved by grain size refinement along with solid-solution and precipitation hardening. A recent development of ferrite-martensite steels, so-called dual phase (DP) steels [1-4] are a special class of microalloyed steels that offer improved formability at the same strength levels. They are obtained by re-heating the HSLA steel in the ferrite-austenite region (intercritical annealing) to develop a structure of about 80% ferrite and 20% martensite (with some retained austenite). These dual phase steels are finding application in several product areas [1] where improved strength/weight ratios and formability are required. Studies of the wear performance of DP steels have not yet been reported; however, certain characteristics (e.g. strength, ductility) of this alloy class suggests the potential for effective wear performance. Several commercial DP steels have been obtained in sheet form for this study. One such alloy (DP 80) will be reported on here; the indicated composition was 0.13% C, 1.56% Mn, 0.63% Si, 0.06% Al, 0.036% V, 0.01% P, 0.01% S, 0.014% Ce, 0.008% N. Wear specimens were machined from this sheet after removing

---

\*Numbers in brackets indicate references.

about 0.1 mm from the surface but were not heat treated prior to testing. The initial microstructure is shown in Fig. 3b.

Tool steel alloys are also used extensively in wear situations and are characterized by high hardness and wear resistance. An oil-hardening tool steel, AISI type O-2, was studied here in both annealed and hardened states. The nominal composition was 0.90% C, 1.6% Mn, and 0.25% Si. This steel is relatively inexpensive and the high carbon content produces good wear resistance in cutting operations that do not involve high temperatures. The material was obtained in bar form; wear specimens were machined from the bar and annealed at 815°C in sealed glass vials. One group of wear specimens was hardened by oil quenching from 802°C followed by tempering for 1 hour at 275°C. The resulting microstructure is shown in Fig. 4.

Two copper-aluminum single phase alloys were obtained for study, Cu-3.5wt%Al and Cu-7.0wt%Al. The alloys were vacuum cast. They were then annealed 3 hours at 800°C and hot rolled from 5.0 to 1.55 cm thickness in 5 passes. Wear block specimens were obtained by machining (fly cutting) from the rolled bar stock.

All wear tests reported here utilized bearing quality AISI type 52100 steel surfaces as the counterfaces. A bearing ball (6.35 mm diameter) was used in the linear tribometer where a new contact area was used for each independent test. Tapered rings (roller bearing cups) were used in the block-ring wear test system. Typically two to four tests were carried out with each ring, although a new ring was used for each change of material or specimen.

### III. Results and Discussion

#### A. *Wear Experiments*

##### 1. Break-in studies

The break-in process, in the context of this report, will be defined as that set of changes in the tribological behavior which occur in a newly established solid contact prior to the establishment of constant average friction coefficient and/or constant wear rate (referred to as "steady state"). Furthermore, a distinction will be made here between friction and wear break-in behavior. The purpose of this phase of the project was to examine the initial stages of microstructural response to applied surface tractions.

The following materials were studied:

- 1) normalized 1015 steel
- 2) dual phase steel (DP 80)
- 3) oxygen free high conductivity (OFHC) copper
- 4) Cu-3.5wt%Al
- 5) Cu-7.0wt%Al

Table I lists basic characteristics of these materials.

Two experimental apparatus were used in determining break-in behavior: the block-on-ring tribometer and the linear tribometer as described earlier. The latter device provided information on the initial friction transients at various locations on the wear track.

##### (a) Linear tribometer results

Pass-by-pass studies were performed in laboratory air on the materials summarized in Table II. Flats were given a final mechanical polish through 1  $\mu\text{m}$  diamond paste the day of the test and both ball and flat were degreased in hexane, acetone and methanol before installation in their



TABLE I. MATERIALS STUDIED IN BREAK-IN TESTS

Material	Condition	Microhardness KHN <sub>200</sub> (kg/mm <sup>2</sup> )	Average Grain Intercept Length (μm)
SAE 1015 steel	Normalized	178±8	49±7
DP-80 steel	As-received	235±8	8±3
OFHC Cu	As-received 5.1 cm round rod	114±5	39±20
Cu-3.5wt%Al	As-received (see text)	131±9	(See Note)
Cu-7.0wt%Al	" "	169±12	(See Note)

## Note:

As-received Cu-Al alloys had a partially (about 50 vol. %) recrystallized microstructure consisting of regions of large grains with deformation twins (exceeding 250 μm diameter) and small recrystallized grains (averaging about 10 μm diameter).

TABLE II. PASS-BY-PASS FRICTION TEST CONDITIONS

Material of Flat	%RH Lab.	Track Number	New or Used Ball	Load (N)	Total No. Passes on Track
1015 Steel	35	1	N	2.5	5
		2	U	2.5	4
		3	N	4.9	9
		4	U	4.9	4
		5	U	2.5	8
DP80	24	1	N	4.9	3
		2	U	4.9	4
		3	N	2.5	13
		4	U	2.5	4
OFHC Cu	52	1	N	4.9	22
		2	N	2.5	57
		3	N	4.9	5
		4	U	2.5	4

test fixtures. Initial surface roughness values were approximately  $0.03 \mu\text{m}$   $R_A$ . Riders were lowered slowly onto the starting point of each pass, the recorder X-axis motion was started and then the table traverse was set in motion.

A typical set of friction traces for 1015 steel is shown in Fig. 5. The general appearance of the traces was similar for all three materials, but the time of development of the larger peaks and troughs as well as the magnitudes of the friction coefficients differed.

Figure 6 compares the maximum value, the minimum value and the difference between maximum and minimum values of friction coefficients for each separate pass for the three materials indicated in tests using a 2.5 N load. As shown, once the friction force began to change the maximum recorded friction climbed rapidly from pass to pass. The DP80 and 1015 steel data also show that the friction range tended to maximize at some point in the transition process. Initial optical studies of wear tracks show that track features at specific positions tended to correspond with specific variations in friction coefficient. For example, smooth-appearing track portions showed less variation in friction coefficient while rapid drops in friction corresponded to areas of the tracks where large debris fragments had become dislodged. Figure 7 is an optical photomicrograph of a portion of the wear track on a 1015 steel specimen where the friction trace showed a marked drop. A portion of the friction trace showing this feature is presented in Figure 7. During the next reporting period such friction behavior will be linked to surface and subsurface microstructural details for linear tests conducted in an argon atmosphere. The present set of linear tribometer "lab air" results will serve primarily as a guide to break-in track development and as an added basis for evaluating argon test results.

## (b) Block-on-Ring Results

These break-in studies were concerned with the analysis of the early portions of the block-on-ring wear - and friction - vs - time curves on all the metals studied. Surface preparation techniques described earlier led to initial surface roughness values in the range of  $0.03 \mu\text{m}$  to  $0.08 \mu\text{m} R_A$ . Two examples of break-in for DP80 steel specimen are shown in Fig. 8. Two features of break-in were of particular interest: 1) the general shape of the friction and wear curves and 2) the time required to reach steady state conditions for friction coefficient and wear rate. Figure 9a depicts four basic friction curve shapes observed for the specimens studied here. Figure 9b shows several curves for the DP80 steel alloy in particular. Table III lists break-in behavior for all materials tested. The friction symbols used in Table III refer to those symbols defined on Fig. 9a. The friction break-in of the five alloys studied are plotted in the histogram in Fig. 10. For Cu-Al alloys the use of previously unworn test rings generally resulted in longer friction break-in periods. However, for the steel specimens this was not always the case.

The friction break-in time is expected to reflect the block and ring interactions including material transfer characteristics, work-hardening, debris accumulation and texturing of the materials. In the case of previously worn ring surfaces, the steady state wear surface microgeometry and surface composition did not require as much time to reform in subsequent tests (even though rings were solvent cleaned with hexanes, acetone and methanol between runs). The behavior of certain steels was not easy to understand. The microstructural features of the

TABLE III. BREAK-IN DATA FOR BLOCK-ON-RING TESTS

BLOCK	New or Used Ring	Test Code	FRICTION COEFFICIENT			Cycles to $\mu_{SS}$	Type of Break-in	Cycles to Constant Wear Rate
			$\mu_0$	$\mu^*$	$\mu_{SS}$			
1015	N	S1-1	.33	-	.67	2290	a	~0
	U	S1-2	.35	-	.80	2020	a	600
	U	S1-3	.28	-	.70	1790	a	370
	U	S1-4	.27	-	.55	1500	a	990
	N	S2-1	.30	-	.65	2310	a	820
	U	S2-2	.32	-	.77	2560	a	1650
	U	S2-3	.39	.60	.82	1810	c	880
DP80	N	DP1-1	.28	.63	.50	820	b	460
	U	DP1-2	.31	.72	.53	550	b	640
	U	DP1-3	.25	.53	.50	450	b	270
	N	DP1-4	.36	.67	.55	1010	b	550
	U	DP1-5	.33	.75	.72	990	d	1650
	N	DP2-1	.32	.34	.51	1500	d	1010
	U	DP2-2	.25	-	.45	1500	a	330
U	DP2-3	.40	.47	.42	910	d	910	
0-2	N	R1	.46	.67	.52	270	b	500
	U	R2	.53	.66	.56	640	b	730
	U	R3	.46	.74	.55	460	b	730
	U	R4	.53	(Note 1)	.55	(Note 2)	(Note 2)	910
Cu-3.5A1	N	3.5A1-1	.34	.50	.86	1650	c	640
	U	3.5A1-2	.26	-	.85	640	a	(Note 3)
Cu-7.0A1	N	7A1-1	.30	.45	.76	1470	d	110
	U	7A1-2	.51	.82	.70	1100	b	(Note 4)
	U	7A1-3	.33	-	.68	500	a	~0

Table Notes:

- (1) See Fig. 9a for definition of friction coefficients.
- (2) No observed break-in in friction trace.
- (3) Erratic wear curve.
- (4) No observed break-in in wear trace.

steel may play a role in this case, and will be a subject of continuing analysis in the next reporting period.

A final observation on the friction and wear break-in lengths is represented by the "break-in map" in Fig. 11. Break-in types indicated for each marked region refer to Fig. 9a. Here, it will be noted that wear and friction break-in periods did not always coincide, and that break-in types and specific materials tended to cluster in certain areas of the map. It should also be noted that data for the 0-2 tool steel, which exhibited the anomalous frictional break-in with new and used rings, lay entirely in the region where wear break-in exceeded friction break-in. The microstructural and surface film implications of the "break-in map" will be further considered as more metallographic studies are carried out on these metals.

## 2. Wear Studies

### (a) Steel alloys

Wear and friction measurements were carried out on the alloys using the block-on-ring tester. The experiments were conducted using a 52100 steel ring as the counterface, 10 N load, and 20 cm/s sliding speed in an argon atmosphere at about 23°C. Sliding distances of either 363 m (1800 seconds time) or 726 m (3600 seconds time) were used. Both new rings and rings previously used for the same alloy were employed and are identified in this discussion.

Examples of the friction curves and wear curves obtained from several experiments on the DP80 steel and the 1015 steel are shown in Figs. 8, 12, and 13. These data show some of the variations encountered in the wear experiment results. Figures 8a and 8b show different trends in the wear

volume change with time. The steady state wear rate on both examples is, however, in agreement as determined from the last 25% to 50% of the run time. While the friction-time curves in these cases are of a similar type, the beginning friction peak in Fig. 8a is more pronounced, possibly reflecting the nature of the break-in processes for this particular specimen-ring combination. The decreasing slope of the wear volume-time curve for early times in Fig. 8a may also result from this same effect. In both curves the depth of the wear scar measured after the experiment was completed is indicated on the wear axis at the point P. A stylus profilometer was used to obtain this value. In this way an absolute measure of wear scar depth is obtained for comparison with the wear depth values obtained during the experiment using the LVDT system. The profilometer measured wear scar depth was usually 10% to 20% greater than that measured by the LVDT system. This difference is attributed to the effect of wear debris in the contact zone and metal transferred to the ring surface, both cases leading to a reduced displacement value measured by the LVDT system.

The results of another experiment using a DP80 steel specimen and a new ring for a longer running time (sliding distance of 726 m) are shown in Fig. 12. The wear curve here is not statistically smoothed before plotting as was done in Fig. 8, and shows the extent of a measured variation in the wear contact position. The wear volume-time curve in Fig. 12 shows a significant transition in slope at about 2400s (480 m sliding distance). The initial wear rate (wear volume per unit sliding distance) is linear but is considerably smaller than the final wear rate. This effect was reproduced in several additional experiments with the DP80 alloy and apparently reflects an actual change in wear process in the

latter portion of the experiments. In view of this finding two average wear rate values are reported for the DP80 steel, one for 360 m sliding distance experiments and one for 720 m sliding distance experiments. This effect was not found for either the 1015 steel or the 0-2 tool steel and will be explored further in order to identify the causes.

Two experimental wear and friction curves for 1015 steel specimens are shown in Fig. 13. In Fig. 13a the wear data are averaged over 5 second intervals for a smoothing effect. Both experiments produced reasonably linear wear volume - time (sliding distance) curves, although both showed a lower wear rate for the initial 300 seconds (60 meters). There was consistent behavior for this alloy in experiments involving the two sliding distances, in contrast to the DP80 steel.

A summary of wear measurements for the 1015 and DP80 steels is shown in the Tables IV and V. The 1015 steel specimens showed fairly consistent friction coefficient and wear rate values. The DP80 steel results indicate a transition in both friction and wear rate over the two distances studied. The wear rate initially (up to 363 m) is about 25% of that found for the sliding distance interval of 363 m to 726 m. The reasons for the sharp transition are not yet understood. The DP80 steel wear rates are significantly lower than those measured for the 1015 steel; a factor of 1/8 to 1/2 lower depending on the sliding distance accumulated. As indicated in Table I the hardness values measured for these two steels are in the ratio



TABLE IV. WEAR AND FRICTION RESULTS ON THE DP80 ALLOY

Sliding Distance (Note 1) (m)	Steady State Friction Coef.	Final Wear Scar Depth ( $\mu\text{m}$ )	Final Wear Vol. ( $\text{mm}^3$ )	Wear Rate (Note 2) ( $\text{mm}^3/\text{m}$ )	Wear Rate from LVDT data (Note 3) ( $\text{mm}^3/\text{m}$ )
363 (N)	0.50	5.4	0.028	$0.77 \times 10^{-4}$	$1.6 \times 10^{-4}$
363	0.55	8.7	0.056	$1.5 \times 10^{-4}$	$1.0 \times 10^{-4}$
363	0.55	8.6	0.055	$1.5 \times 10^{-4}$	$0.72 \times 10^{-4}$
363	0.55	7.1	0.041	$1.1 \times 10^{-4}$	$0.87 \times 10^{-4}$
363	0.55	6.5	0.036	$0.99 \times 10^{-4}$	$0.68 \times 10^{-4}$
avg.	0.55	7.4	0.044	$1.2 \times 10^{-4}$	$0.97 \times 10^{-4}$
726 (N)	0.80	27	0.30	$4.1 \times 10^{-4}$	$5.8 \times 10^{-4}$
726 (N)	0.80	29	0.34	$4.7 \times 10^{-4}$	$7.5 \times 10^{-4}$
726	0.75	28	0.32	$4.4 \times 10^{-4}$	$6.2 \times 10^{-4}$
avg.	0.78	28	0.32	$4.4 \times 10^{-4}$	$6.5 \times 10^{-4}$

Notes:

- (1) N signifies new ring.
- (2) Final wear volume/sliding distance.
- (3) Average over last one-third of experiment.

TABLE V. WEAR AND FRICTION RESULTS ON 1015 STEEL

Sliding Distance (Note 1) (m)	Steady State Friction Coef.	Final Wear Scar Width ( $\mu\text{m}$ )	Final Wear Vol. ( $\text{mm}^3$ )	Wear Rate (Note 2) ( $\text{mm}^3/\text{m}$ )	Wear Rate from LVDT data (Note 3) ( $\text{mm}^3/\text{m}$ )
363 (N)	0.65	20	0.19	$5.3 \times 10^{-4}$	$2.9 \times 10^{-4}$
363	0.80	27	0.31	$8.4 \times 10^{-4}$	$8.7 \times 10^{-4}$
363	0.72	30	0.36	$9.8 \times 10^{-4}$	$9.9 \times 10^{-4}$
363	0.80	22	0.22	$6.2 \times 10^{-4}$	$9.5 \times 10^{-4}$
avg.	0.74	25	0.27	$7.5 \times 10^{-4}$	$7.75 \times 10^{-4}$
726 (N)	0.76	33	0.41	$5.7 \times 10^{-4}$	$6.7 \times 10^{-4}$
726	0.83	56	0.91	$12.5 \times 10^{-4}$	$14.5 \times 10^{-4}$
avg.	0.80	45	0.65	$9.0 \times 10^{-4}$	$10.6 \times 10^{-4}$

Notes:

- (1) N signifies new ring.
- (2) Final wear volume/sliding distance.
- (3) Average over last one-third of experiment.

$HK(DP80)/HK(1015) = 1.32$  for annealed material (and 1.14 for deformed material, measured using tensile specimens, see Table IX later). Hence, the hardness ratios are not sufficient to account for the observed wear rate ratios.

Scanning electron microscope studies have been carried out on the worn surfaces and on debris particles recovered from the steel specimen wear tests. A schematic representation of the block-on-ring geometry is shown in Fig. 14 for use in this discussion. Examples of debris particles recovered as they fell from the 1015 steel block during wear experiments are shown in Fig. 15. Generally, two types of particles are found; large flat particles such as (A) and much smaller, equiaxed particles. Figure 16 shows other examples of this wear debris. In the lower photograph one of the large, flat particles (A) appears to be partly fractured. The smaller particles (less than  $1 \mu\text{m}$  in size) are frequently found clinging to the larger particles and also clumped themselves into a larger aggregate such as at (B). Examination of the entrance zone of the wear scar on the block revealed a similar collection of debris particles. The exit zone of the wear scar on the block showed a different morphology as indicated in Fig. 17. The lower half of Fig. 17a is a portion of the wear scar while the upper half is unworn, original surface. There is some plastic flow of the steel out of the wear scar region causing the irregular edge, approximately perpendicular to the sliding direction (shown by the arrow). One of the plastically deformed protrusions is seen in more detail in Fig. 17b. Clearly some evidence is present suggesting tearing of this material at the edges formed during the microdeformation process. Stereo scanning electron microscope studies of the morphology present provided convincing evidence for debris formation at many of these protrusions.

Studies of the wear scar surface within the contact zone also revealed evidence for considerable plastic deformation. Figure 18 shows two regions (A) within the wear scar where particles of size  $3\ \mu\text{m}$  to  $10\ \mu\text{m}$  appear to be forming by a partially ductile tearing process. Stereo-viewing of micrographs taken from the wear scar region suggests that the normal load at any time is carried by only a small fraction of the apparent area and that plastic flow both in the direction of sliding (arrow) and transverse to that direction is probably significant in forming the ridges and lips of material, as well as forming debris particles.

Wear debris was also recovered from experiments involving the DP80 alloy. One collection of particles is shown in Fig. 19. Three different classes of particles were found; further details are presented in Fig. 20. Relatively large flat particles (A) were found that frequently show crack-like features (arrows). Comparably large particles of a distinctly different morphology (B) were also found. Further, much smaller ( $< 1\ \mu\text{m}$ ) wear particles of roughly equiaxed dimensions were always present. One area in the entry region of the wear scar is shown in Fig. 21a. Wear debris particles found in that region (Fig. 21b) were similar to those recovered after falling from the wearing contact. Again score lines and crack-like features are seen (A). The morphology at the exit side of the wear scar is seen in Fig. 22. There is considerable evidence for plastic flow of material. In Fig. 22b, the lip of metal shown has numerous crack-like features at the edges as well as transverse ripple markings that suggest constrained plastic deformation. Studies using stereo scanning electron microscopy of the wear scar surface within the contact zone (such as Fig. 23) showed that the normal load was probably carried by a

small fraction of the apparent area as evidenced by flat ridges of metal (A) extended in the sliding direction. Irregular edges of these ridges were commonly found. In most of the micrographs obtained, the surface regions within the contact zone that were depressed away from contact with the ring surface appear to have collected quantities of the small debris particles (such as at B in Figs. 22a, 23). This process of fine debris collection and compaction within the wear gap may in fact produce the porous appearing debris particles typified by the example in Fig. 20b. Similar features were observed on the wear scars on the copper-aluminum blocks to be discussed next.

#### (b) Copper alloys

Wear and friction measurements were carried out on the Cu-3.5wt%Al specimens and the Cu-7.0wt%Al specimens. The first tests on each alloy used a new 52100 steel ring; subsequent tests of each alloy were conducted using the same ring after ultrasonic cleaning (in acetone and methanol). Table VI summarizes the Cu-Al test results. With the exception of the last test of Cu-7.0wt%Al which ran twice as long as the others, all tests were performed under similar conditions. Figure 24 shows a representative wear and friction plot for one of these alloys. As shown in Table VI, steady state sliding friction was lower for the higher Al content. Initial frictional behavior was discussed in the section dealing with break-in studies. Based on the data in Table VI it is found that higher aluminum content led to higher wear volume and wear rates. Further, the alloys with lower friction coefficients also had higher wear values.

TABLE VI. WEAR AND FRICTION RESULTS FOR THE Cu-Al ALLOYS

Alloy (wt%Al)	Sliding Distance (Note 1) (m)	Steady State Friction Coef.	Final Wear Scar Depth ( $\mu\text{m}$ )	Final Wear Vol. ( $\text{mm}^3$ )	Wear Rate (Note 2) ( $\text{mm}^3/\text{m}$ )	Wear Rate from LVDT data (Note 3) ( $\text{mm}^3/\text{m}$ )
3.5	363 (N)	.87	4.3	.114	$3.1 \times 10^{-4}$	(Note 4)
	363	.85	3.7	.105	$2.9 \times 10^{-4}$	(Note 4)
	avg.	.86	4.0	.110	$3.0 \times 10^{-4}$	-
7.0	363 (N)	(.7)*	27.5	.288	$8.0 \times 10^{-4}$	$2.6 \times 10^{-4}$
	363	.70	25.0	.280	$7.6 \times 10^{-4}$	$4.6 \times 10^{-4}$
	726	.68	37.5	.341	$4.7 \times 10^{-4}$	$3.1 \times 10^{-4}$
	avg.	.69	-	-	$6.8 \times 10^{-4}$	$3.4 \times 10^{-4}$

\*Still decreasing slightly at the end of the test.

Notes:

- (1) N signifies new ring.
- (2) Final wear volume/sliding distance.
- (3) Average over last one-third of experiment.
- (4) Erratic.

Specimens of the Cu-Al alloys have been examined by optical microscopy and SEM. Such studies can help clarify the fracture processes involved in debris formation and establish the role of debris in promoting further surface degradation.

Figure 14 showed a typical block wear scar schematically. It is appropriate to discuss the observations made on these alloys in the context of the three zones shown; entrance, contact and exit. Some features of these regions in the Cu-Al alloys are delineated below.

Entrance zone:

Powdery debris which is carried by the turning ring is deposited here and compressed into compacts with varying degrees of mechanical strength. Compacts closer to the scar tend to be stronger. Figure 25a shows this zone on a Cu-7Al specimen. Most loose debris came free upon probing with a camels-hair brush leaving the island near the center of the view. Figure 25b shows the leading edge of the island which may be a region where micrometer-sized debris are trapped and compacted into the island mass. Beneath the looser debris (not present on this sample any longer) there is localized cratering of the flat surface showing an appearance similar to that observed in erosive wear. The possibility of a small additional contribution to wear in the block-on-ring geometry by particles generated ahead of the main scar should be considered based on this evidence.

Contact zone:

The main contact zone of the scars consisted of deep grooving with occasional darker appearing patches covering the grooves. The patches

(see Fig. 26) were often gray with some brighter metallic areas. Preliminary cross-sectioning indicates that they may be "marble cake"-like compacts of oxide and metal. Further metallography is planned to examine the role of oxides. Various bands of color (i.e. black, orange-brown, coppery and bulk alloy colored) were observed by naked eye lying in the direction of sliding. Their widths and location across the scars varied from test to test.

Exit zone:

Evidence for the significance of subsurface deformation in wear was observed in this zone where extensive slip line fields appeared. As shown in Fig. 27a, the surface distortions followed the wear groove pattern closely and extended about 50 micrometers beyond the contact interface. Fig. 27b shows some additional details of the parallel slip line morphology in this region on the Cu-7.0wt%Al, low stacking fault energy, alloy.

Initial results concerning the subsurface structure for a Cu-7.0wt%Al worn block are shown in the photomicrographs in Fig. 28. Figure 28a shows a longitudinal cross section (sliding direction right to left) of a wear surface in the polished, unetched condition (copper plated before sectioning). The dark gray regions at the copper plating/sample interface have the appearance of a "marbleized" mechanical mixture of bright metal and oxide debris. This is consistent with the mottled appearance of patches observed on the sliding surface of this alloy. Light etching\* by swabbing revealed the thin (approximately 4  $\mu\text{m}$ ) deformed layer below the sliding surface (Fig. 28b), but it also resulted in a loss of interface material and oxide-metal details.

---

\*2 g  $\text{K}_2\text{Cr}_2\text{O}_7$ , 1.5 g NaCl, 18 ml  $\text{H}_2\text{SO}_4$ , 100 ml  $\text{H}_2\text{O}$ .



This phenomenon was discussed in a recent paper by Ahn et al. [6]. Further subsurface studies are planned for the other wear tested materials. Characterization of the dimensions and structure of such sliding wear-deformed constituents is felt to be central to developing a valid structure/properties relation for friction and wear.

#### B. *Mechanical Properties Measurements*

Measurements have been carried out on 1015 steel and the DP80 steel specimens to determine certain bulk mechanical properties that may be relevant to the wear characteristics of those alloys. Figure 29 shows the configuration of the tensile specimens used in these experiments. The relevant dimensions are listed in Table VIII. True stress-true strain analysis of the data from these tensile tests was carried out in order to obtain strain hardening coefficients for the two materials studied. According to this analysis, the stress-strain relation

$$\sigma = K \epsilon^n$$

is fitted to the observed data, as shown in Fig. 30 for one specimen. This method derives two parameters, K, the strength coefficient, and n, the strain-hardening coefficient, that describe the plastic response of the material to uniaxial tensile loads. A summary of the results are shown in Fig. 31 and Table VIII.

The lower value of strain hardening coefficient measured for the DP80 steel is characteristic of such materials. While the yield stress of the DP80 steel is only slightly greater than that for the 1015 carbon steel (353 MPa vs 309 MPa, respectively, about 14%), the tensile strengths differed considerably (682 MPa vs 500 MPa, about 36%). This increased

TABLE VIII. TENSILE DEFORMATION RESULTS ON STEELS

Material	Description	Yield stress (MPa)	Tensile Strength (MPa)	Reduction in area at fracture (%)	Coefficient	Strain hardening Exponent
1015	L	304	507	32	900	0.22
1015	L	314	493	30	900	0.23
avg	-	309	500	31	900	0.23
DP80	L	355	704	47	1160	0.19
DP80	L	352	673	54	1060	0.17
DP80	T	355	669	42	1120	0.19
DP80	T	352	680	53	1120	0.19
avg	-	353	682	49	1110	0.18

All specimen gage section 2.54 cm long, 1.5 mm wide, 2 mm thick (DP80) or 3 mm thick (1015).  
 (Specimens are sub-standard size).

L = longitudinal orientation; T - transverse orientation.

strength level arises from the hardening effect of the microalloyed solutes rather than the carbon content which is actually slightly reduced in the DP80 steel. Equally significant is the increased ability of the DP80 steel to withstand greater reductions in area than the plain carbon steel (about 58% greater, see Table VIII).

Microhardness measurements were carried out on both these steels and on the 0-2 tool steel; the results are shown in Table IX. Considering first the values for the annealed specimens, the DP80 steel and the 0-2 tool steel showed comparable microhardness values. Both were about 32% greater than that measured for the 1015 carbon steel. This difference was reduced by about 1/2 for the deformed materials. Grain intercept lengths were measured for all three steels and are shown in Table IX. The DP80 steel has a significantly smaller grain size which probably contributed to the higher yield stress values.

While these tensile measurements were obtained under uniaxial tensile loading conditions, and the microscopic deformation conditions at wearing contacts are almost certainly multiaxial with both tensile and compressive components, it is interesting to compare the differences in mechanical behavior of the steels with their measured wear performance. The comparison between DP80 steel and the 1015 carbon steel indicates that both the higher tensile strength values and the greater potential ductility of DP80 steel probably contribute to its greater wear resistance, since plastic deformation effects have been shown earlier to be a prominent feature of the wear process. Tensile data were not obtained for the 0-2 tool steel; however, the microhardness measurements suggest comparable strength levels

TABLE IX. MICROHARDNESS RESULTS ON STEELS

Metal	Description	Grain Intercept Length ( $\mu\text{m}$ )	Hardness Knoop (500 g)	$\frac{\text{Hardness (DP80)}}{\text{Hardness (metal)}}$
1015	annealed	49 $\pm$ 7	178 $\pm$ 8	1.32
1015	deformed	-	244 $\pm$ 10	1.14
DP80	annealed	8 $\pm$ 3	235 $\pm$ 8	1
DP80	deformed	-	279 $\pm$ 10	1
0-2	annealed	30 $\pm$ 7	233 $\pm$ 5	1.01

with DP80 steel. The somewhat greater wear resistance of the DP80 steel relative to the 0-2 tool steel that was previously described may be due principally to the greater ductility of DP80 steel. Additional mechanical properties measurements on the steels are planned to further explore this matter. Multiaxial deformation data will be sought since such conditions are more closely related to the conditions in the wearing contact.

#### IV. Summary and Plans

Initial results are presented on the wear of three steels and two copper-aluminum alloys. The wear experiments were carried out in two ways: first, the break-in wear and friction processes were studied using a linear ball-on-flat system and a block-on-ring wear system, and second, the steady-state wear processes were studied using a computer-interfaced block-on-ring system.

The break-in studies were designed to examine trends in friction coefficient and worn surface morphology on a pass-by-pass basis for the first 10 to 50 passes for the alloys. Rapid changes in friction values were measured and in some cases correlated with changes in wear track morphology. In longer time experiments, four types of characteristic friction curves were identified. The number of cycles (distance of sliding) that were required to achieve constant friction or constant wear response were measured and compared among the alloys using a "map" representing friction vs wear break-in behavior. Each of the alloy systems produced data that clustered in particular regions of this map. This is interpreted to result from a characteristic combination of significant parameters such as oxide type and thickness, subsurface

deformation modes, and to an unknown extent the kinetic relations between the mechanical and chemical processes involved.

Steady-state wear studies were carried out for total sliding distances of both 363 m and 726 m. Wear depth values were obtained continually (2 Hz rate) through the course of each experiment using the LVDT system. In this way the time periods required for steady state wear could be determined and changes in wear rate during the experiment could be measured. In all experiments the generation of wear debris and the transfer of metal and oxide between the contacting surfaces was noted. Accumulation of debris at the entrance edge of the wear scar was a major factor. In approximate terms about one-half of the debris typically fell from the block-ring combination onto the debris collecting surface, the balance remaining on the ring or block. Microscopic studies of the contacting surfaces after the experiments showed evidence for wear debris accumulation within the contact gap at locations where surface depressions existed.

Three characteristic types of wear debris particles were identified. Flat metallic particles were prominent in the debris with major axis dimensions from about 1  $\mu\text{m}$  to 40  $\mu\text{m}$  and thicknesses up to about 1  $\mu\text{m}$ . Examination of the worn surfaces revealed many features resulting from plastic deformation both within the contact gap and at the exit end of the wear scar. The size and features of these deformed ridges and lips suggested that production of flat debris particles could be explained by ductile failure processes on a microscopic scale. A second type of large particle was clearly the result of compaction of much smaller particles, presumably occurring within the contact gap or possibly at the entrance edge. The third type were small particles about 0.1 to 1  $\mu\text{m}$  in all dimensions that may have been formed by elementary rubbing processes between the surfaces. These smallest particles were compacted into one type of the

larger particles as noted above. Xray diffraction studies have been initiated to identify the oxides and metals present in the wear debris collections since it seems plausible that the smallest particles are largely composed of oxides.

The wear rate measurements of the two types of steels revealed some interesting differences. In particular, the DP80 steel wear rate while initially about 1/8 that of the 1015 steel, increased for longer sliding distances until it was about 1/2 that of the 1015 steel. Clearly a change of this magnitude reflects a change in the dominant wear process. The measured coefficients of friction as well showed a corresponding change for the DP80 alloy. The two copper alloys also showed significant trends in both friction coefficient and wear rate. The wear rate doubled with a two-fold increase in aluminum concentration while the steady-state friction coefficient decreased with that change. No particular trends with composition in the principal wear debris particle characteristics were noted, but further studies into this question are in progress.

The mechanical properties measurements on the two steels revealed some significant differences that were generally expected. The DP80 steel alloy exhibited a slower work-hardening rate than that for the 1015 carbon steel specimens under uniaxial tensile deformation. The greater formability of the DP80 alloy is consistent with in such behavior. In contrast, the microhardness values for the 1015 steel in the deformed condition were only about 15% lower than for the DP80 alloy. Thus the difference in microhardness is probably only a small factor in the overall difference in mechanical behavior of the two types

of steel and hence in the contrasting wear resistance.

Plans for the coming year in this project include the following studies:

- two other dual phase steel alloys will be examined in terms of wear behavior and mechanical properties.
- microstructural studies of subsurface regions in worn specimens will be emphasized.
- friction and wear break-in characteristics will be determined for the alloys in different environments, particularly studying the effect of water vapor and contaminants.
- an oil-free, ultrahigh vacuum pumpable wear system will be constructed for studies in various controlled atmospheres.
- compression testing and multi-axial mechanical testing of the different steels will be conducted for comparison with wear performance.
- the complex wear rate characteristics of the DP80 alloy will be closely examined.
- relevant wear mechanism differences among the iron-based and copper-based alloys will be studied.
- the responsible wear debris formation processes in the alloys will be further defined.

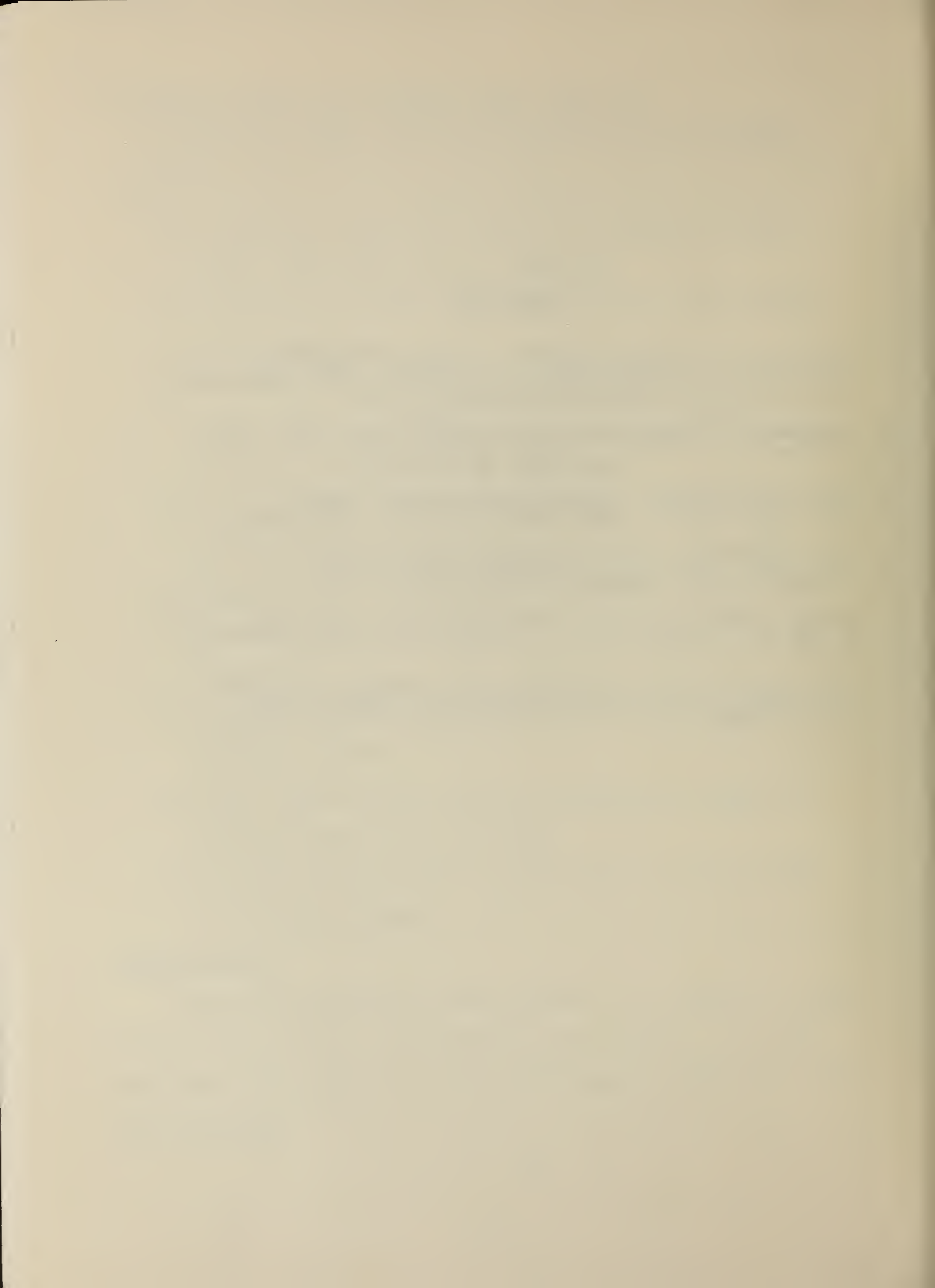
#### Acknowledgements

Considerable assistance has been provided in the experimental phases of this work by Paul Boyer, David Cooper and Kirk Mettam. The copper alloys used in this research were obtained through the cooperation of the Olin Corporation.



### References

1. "A Review of the Status, Selection and Physical Metallurgy of High-Strength, Low-Alloy Steels", E. E. Fletcher, MCIC Report #79-39 (Battelle Columbus Laboratory, Ohio, March 1979).
2. "Molybdenum in Intercritically Annealed Dual-Phase Steel Strip", J. Morrow and G. Tither, J. Metals 30, 16 (1978).
3. "Physical Metallurgy of Automotive High-Strength Steels", R. G. Davies and C. L. Magee, AIME publication in press, 1979.
4. "Dual-Phase Sheet Steels for Automotive Applications", T. Furukawa, Metal Progress 116, 36-39 (1979).
5. Mechanical Metallurgy, G. E. Dieter (McGraw-Hill Book Company, 1961) p. 243.
6. "Metallographic Techniques for Wear Test Specimens", T. M. Ahn, P. J. Blau, K-L Hsu, D. A. Rigney and J. D. Schell, Wear 56, 409-413 (1979).



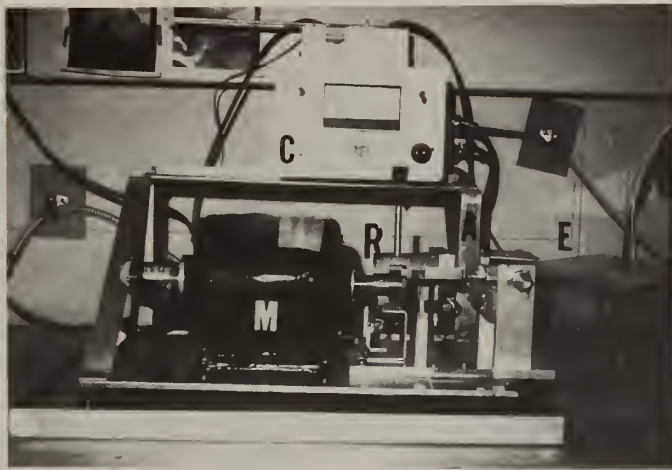


Fig. 1. Wear test apparatus showing motor (M), ring (R), controller (C), specimen arm (A), enclosure (E).

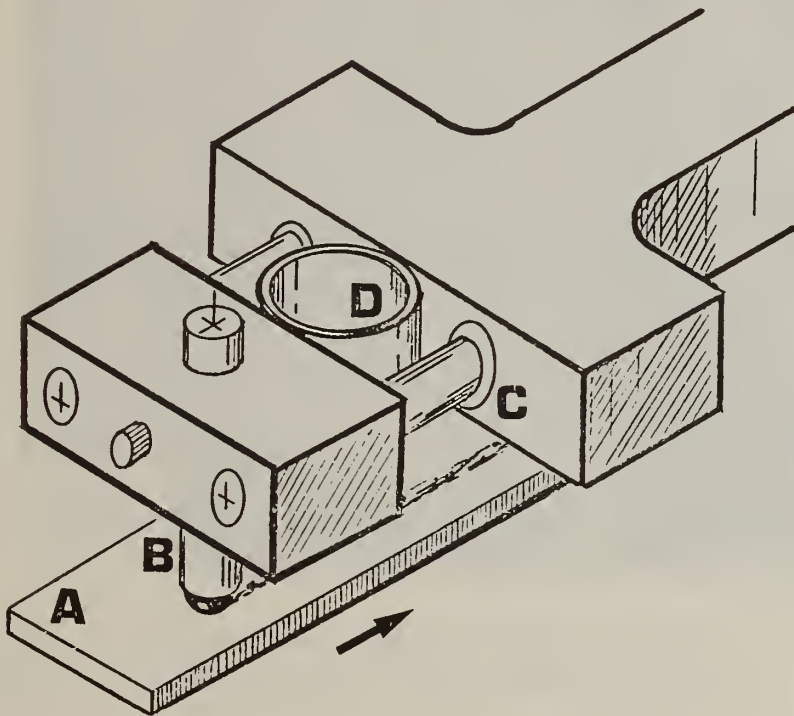


Fig. 2. Schematic of the linear tribometer head: (A) specimen, (B) ball rider on a brass stub, (C) precision linear ball bushing, (D) strain ring with gauges .

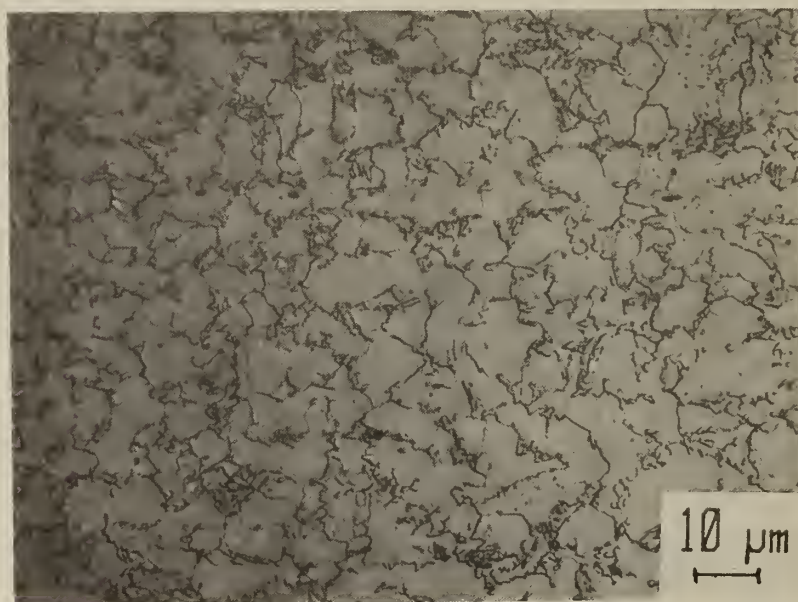


Fig. 3. (a) 1015 steel microstructure, etched in nital,  
(b) DP80 steel microstructure, etched in nital.



Fig. 4. 0-2 tool steel microstructure, etched in nital.

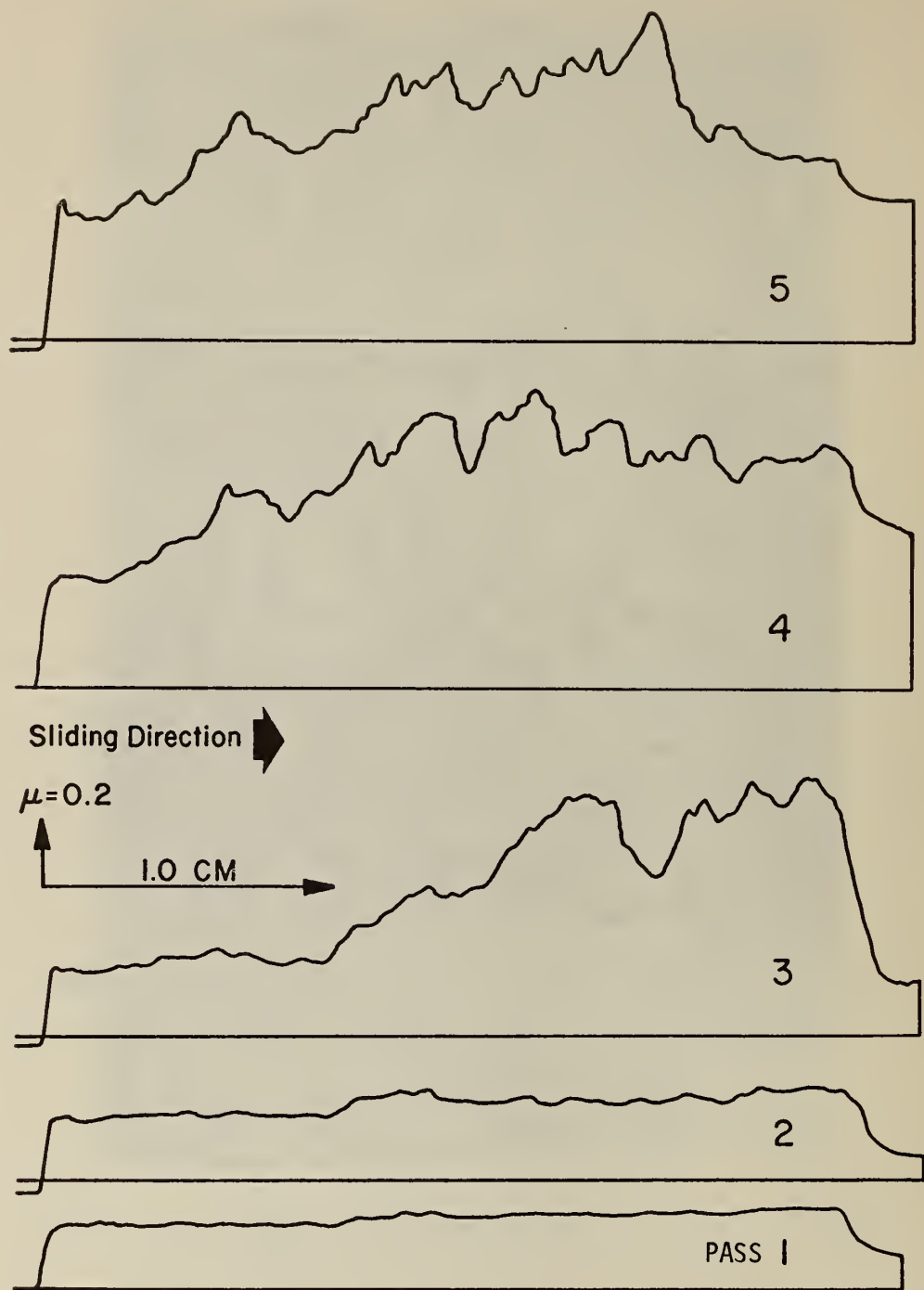


Fig. 5. Observed variation of friction with position on track during the first 5 passes on 1015 steel specimen.

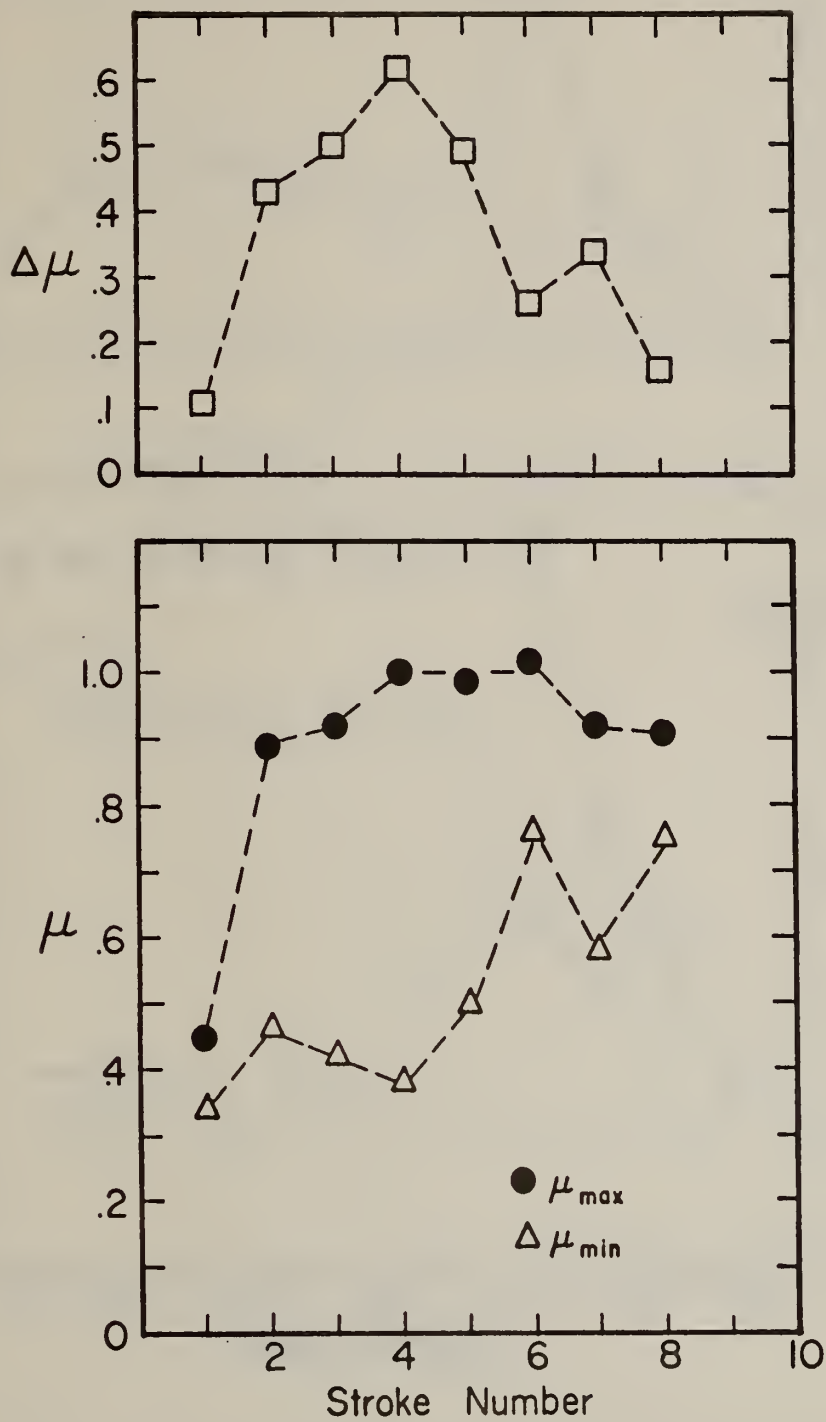


Fig. 6. (a) Linear tribometer friction results for a 1015 steel specimen.

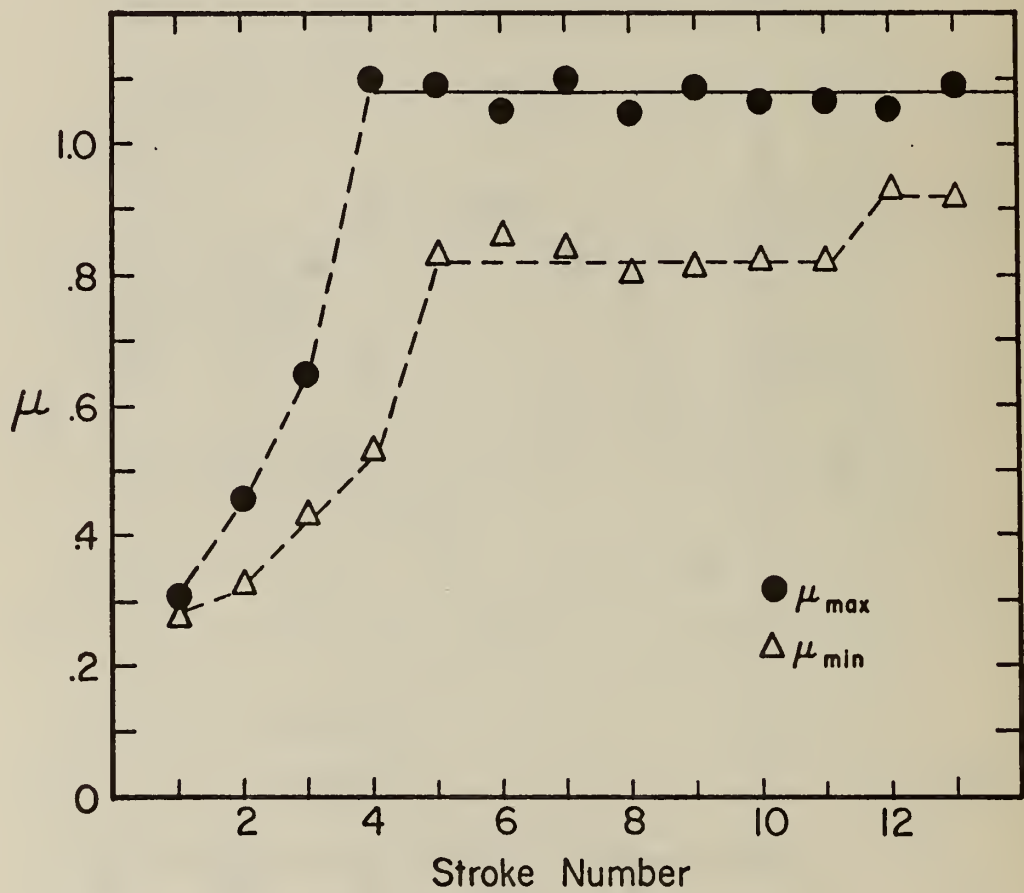
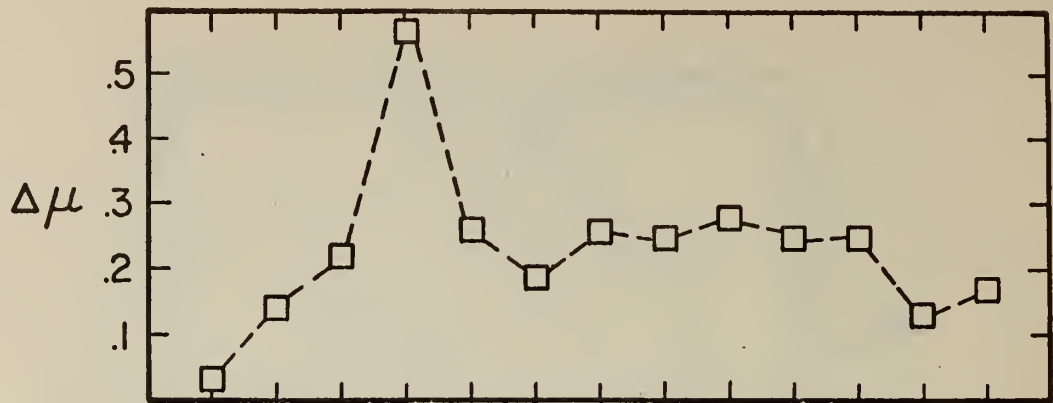


Fig. 6. (b) Linear tribometer friction results for a DP80 steel specimen.



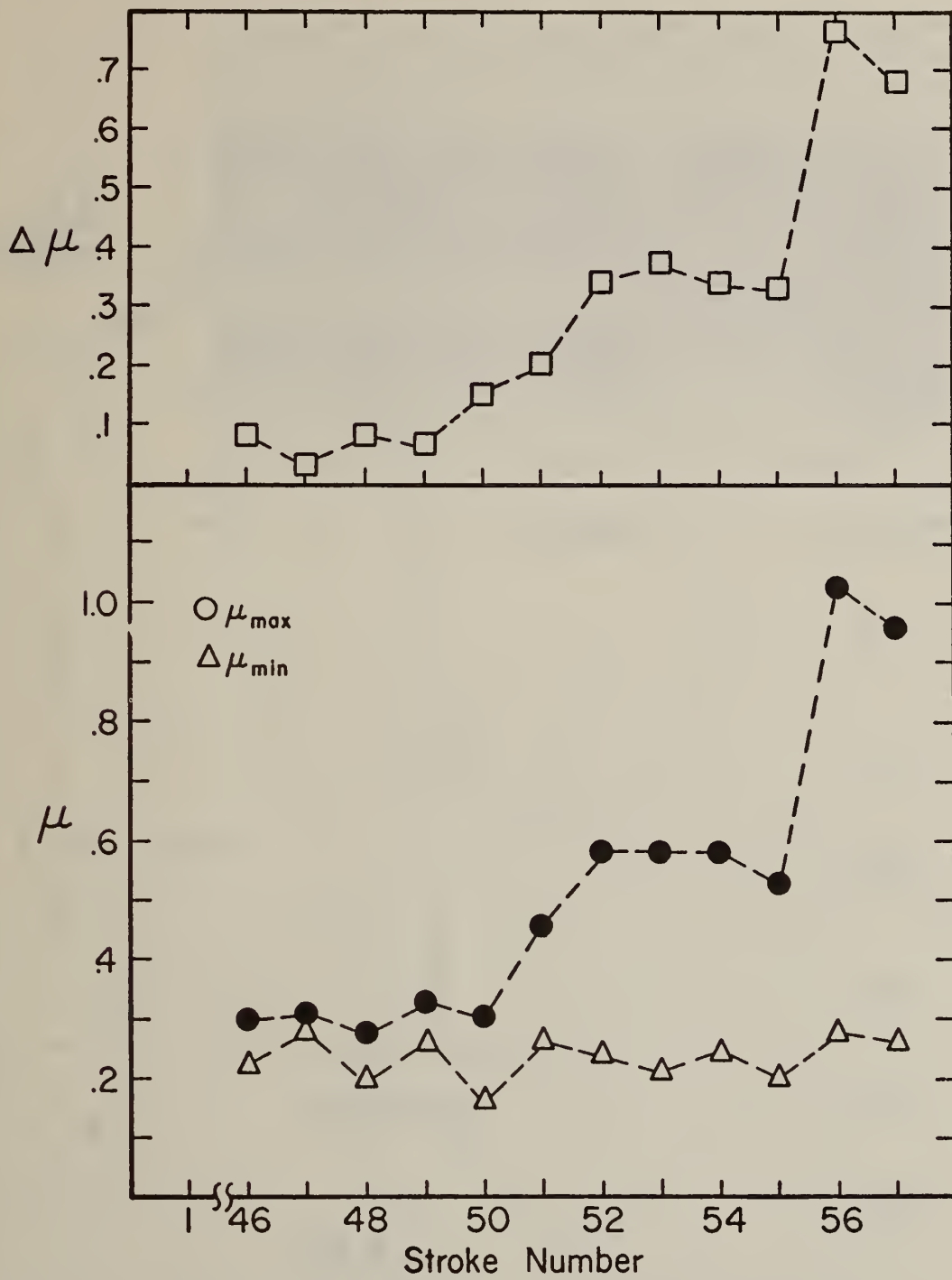


Fig. 6. (c) Linear tribometer friction results for a copper specimen.

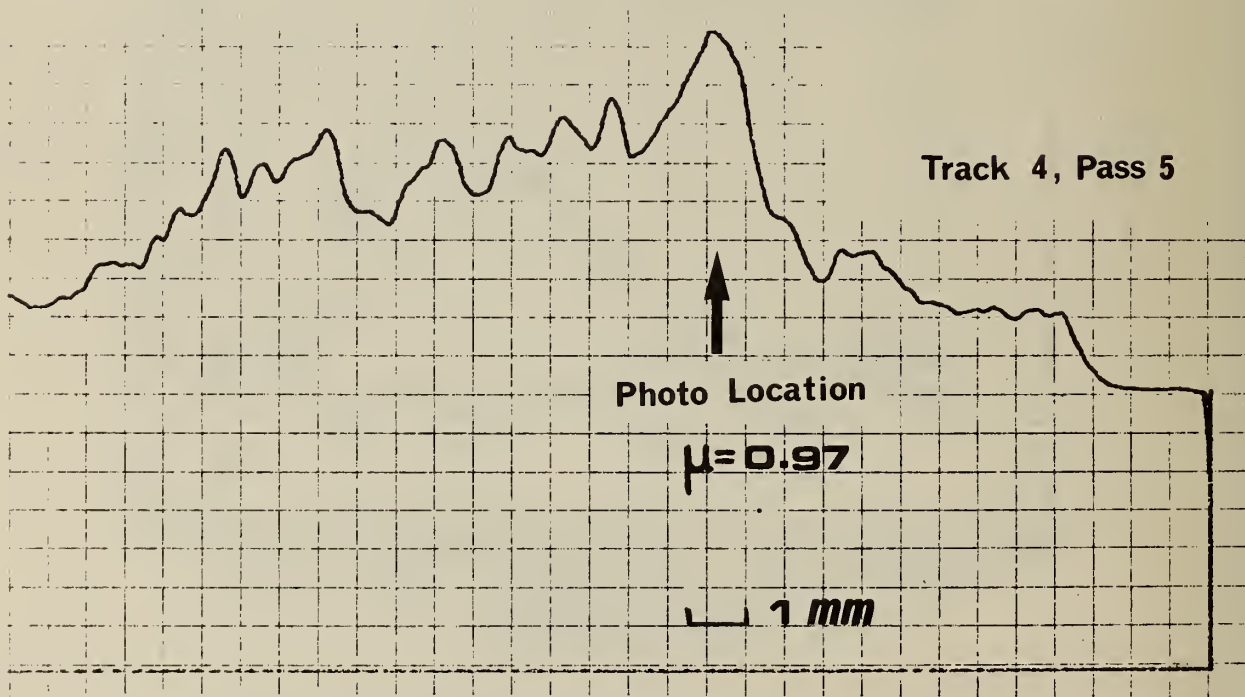
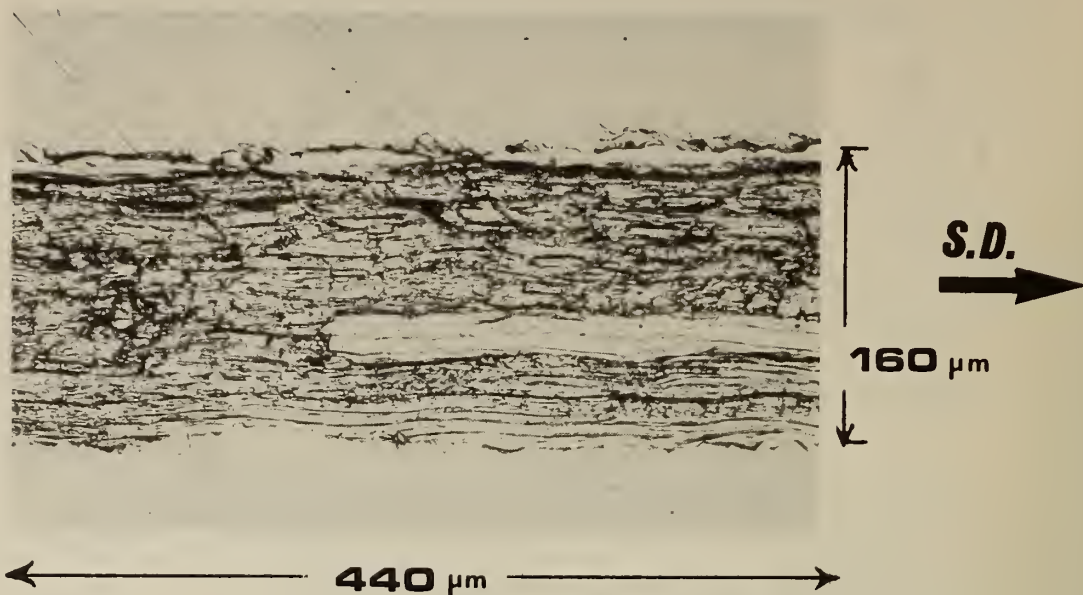


Fig. 7. Optical photomicrograph and friction trace for a 1015 steel specimen. Note the correspondence between a drop off in friction and the beginning of a deep groove in the wear track.

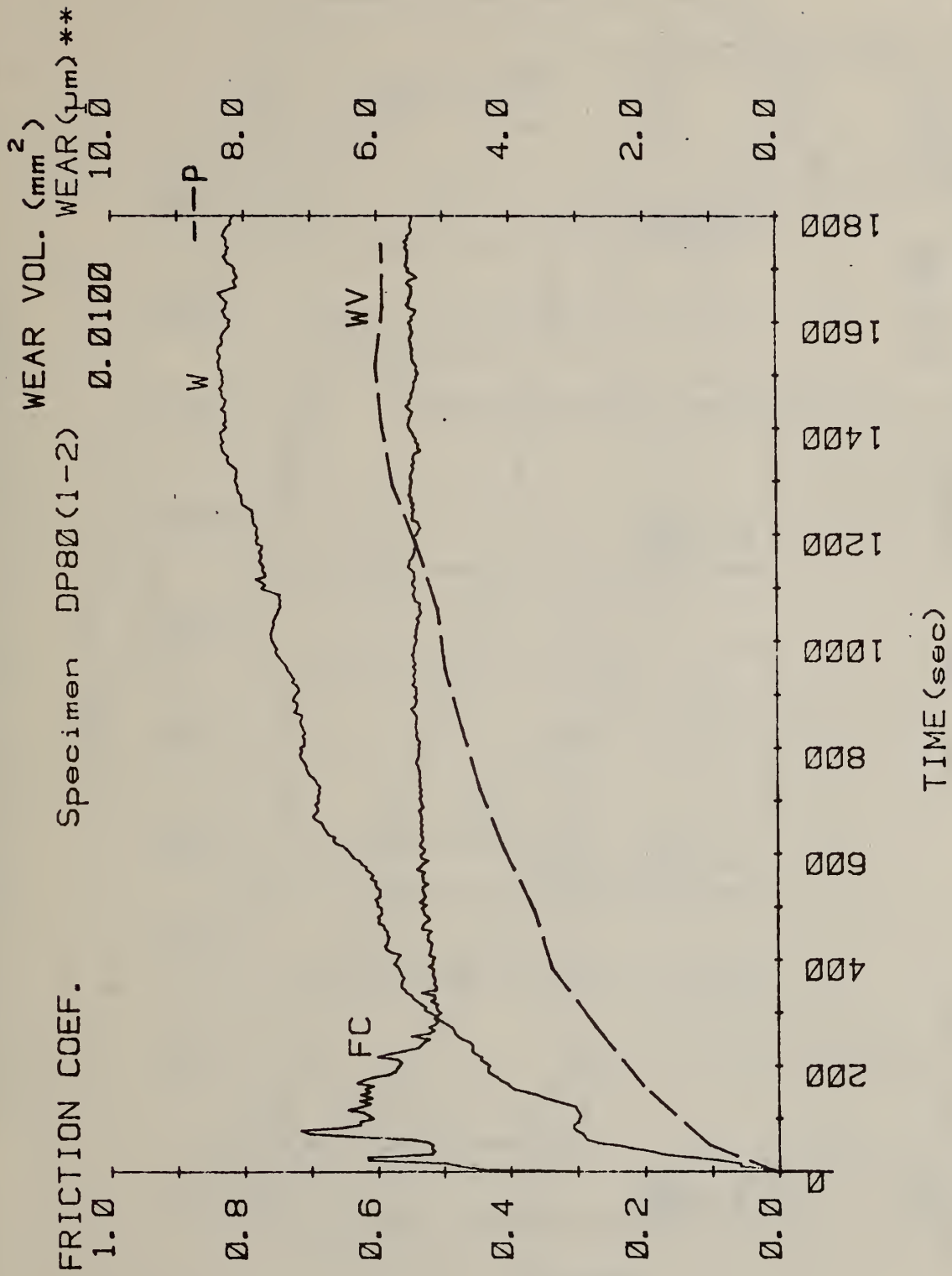


Fig. 8. (a) Wear depth (W), wear volume (WV) and friction coefficient (FC) results for DP80 steel specimen.

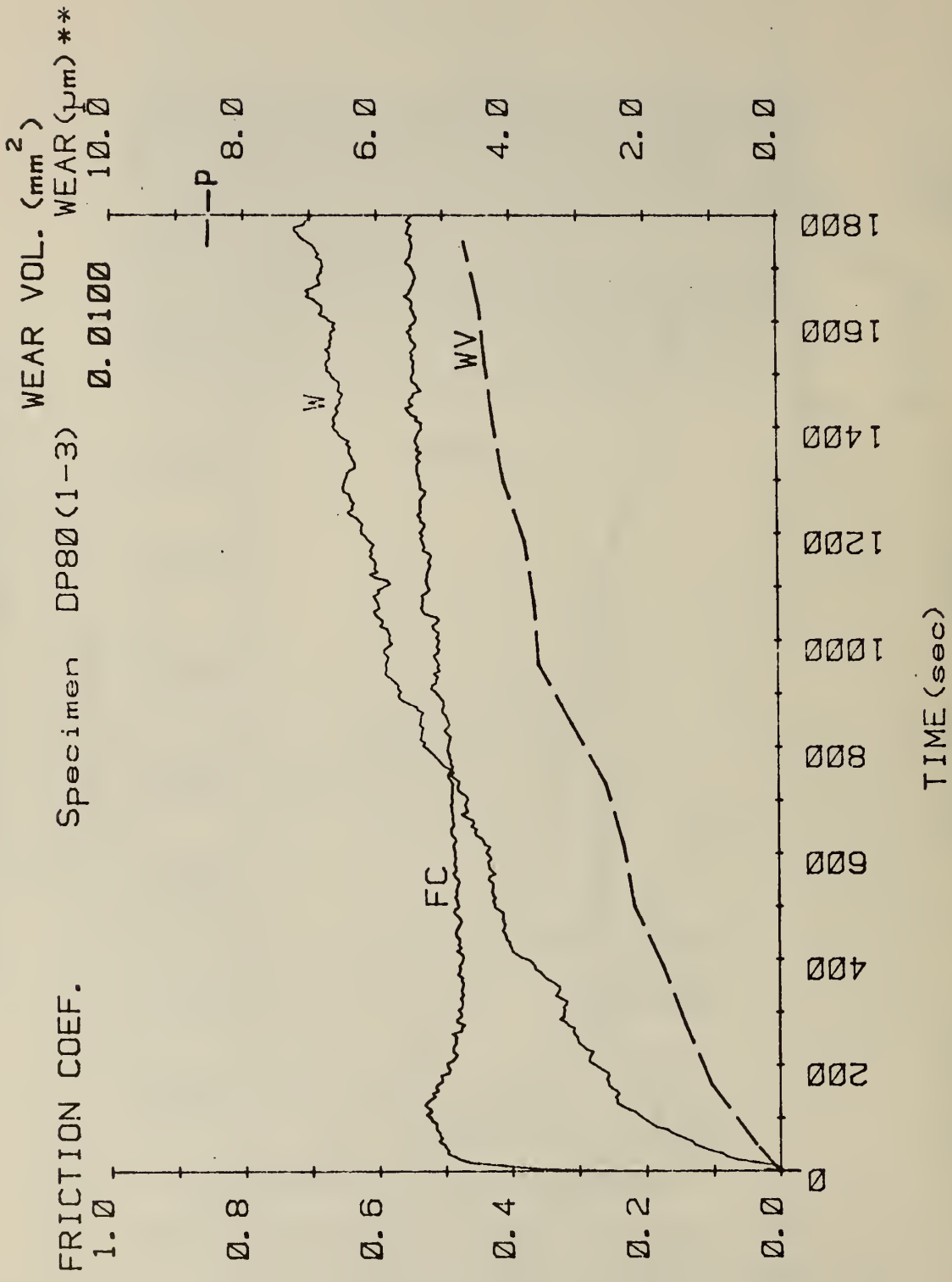


Fig. 8. (b) Wear depth (W), wear volume (WV) and friction coefficient (FC) results for DP80 steel specimen.

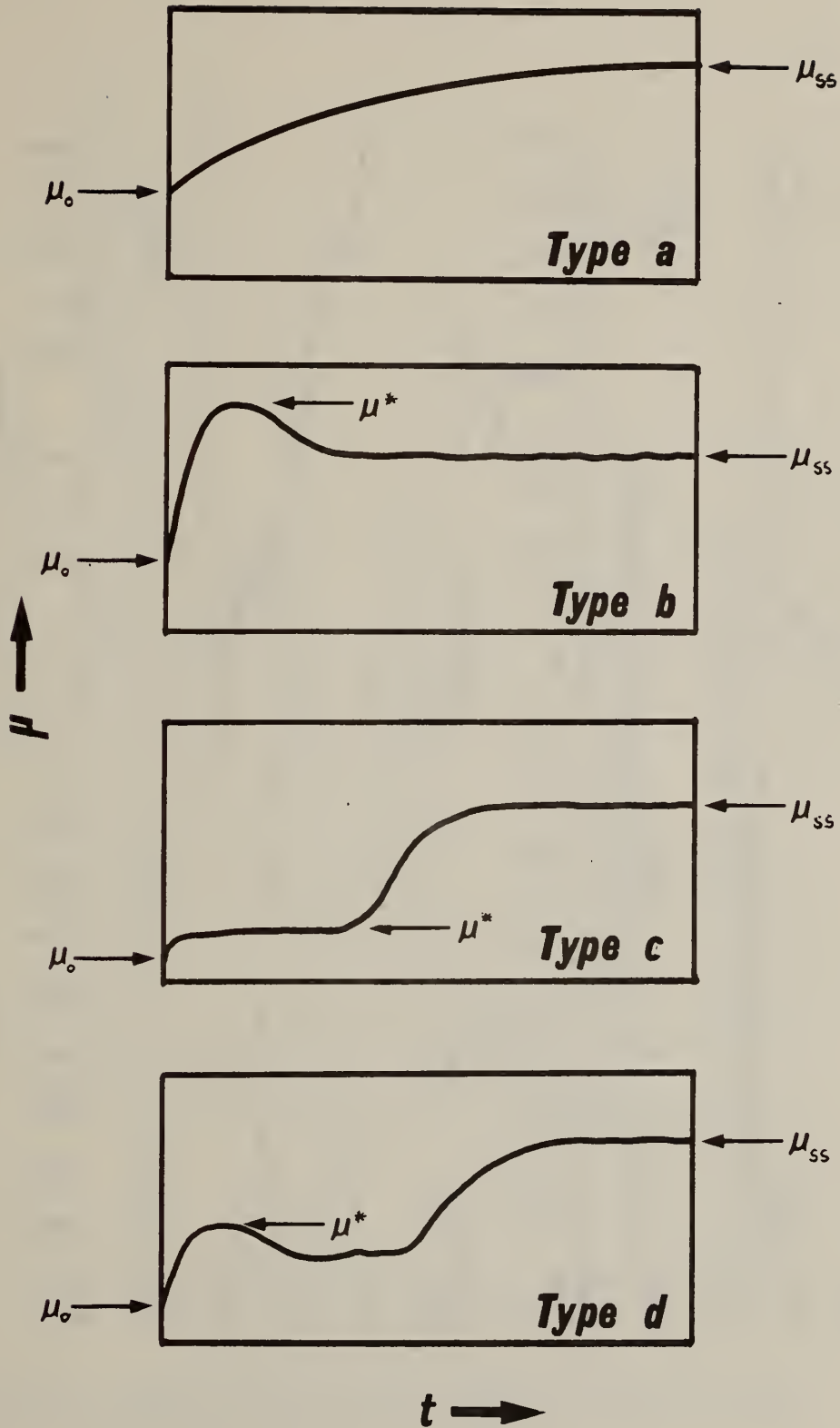


Fig. 9. (a) Types of friction break-in curves observed for block-on-ring tests.

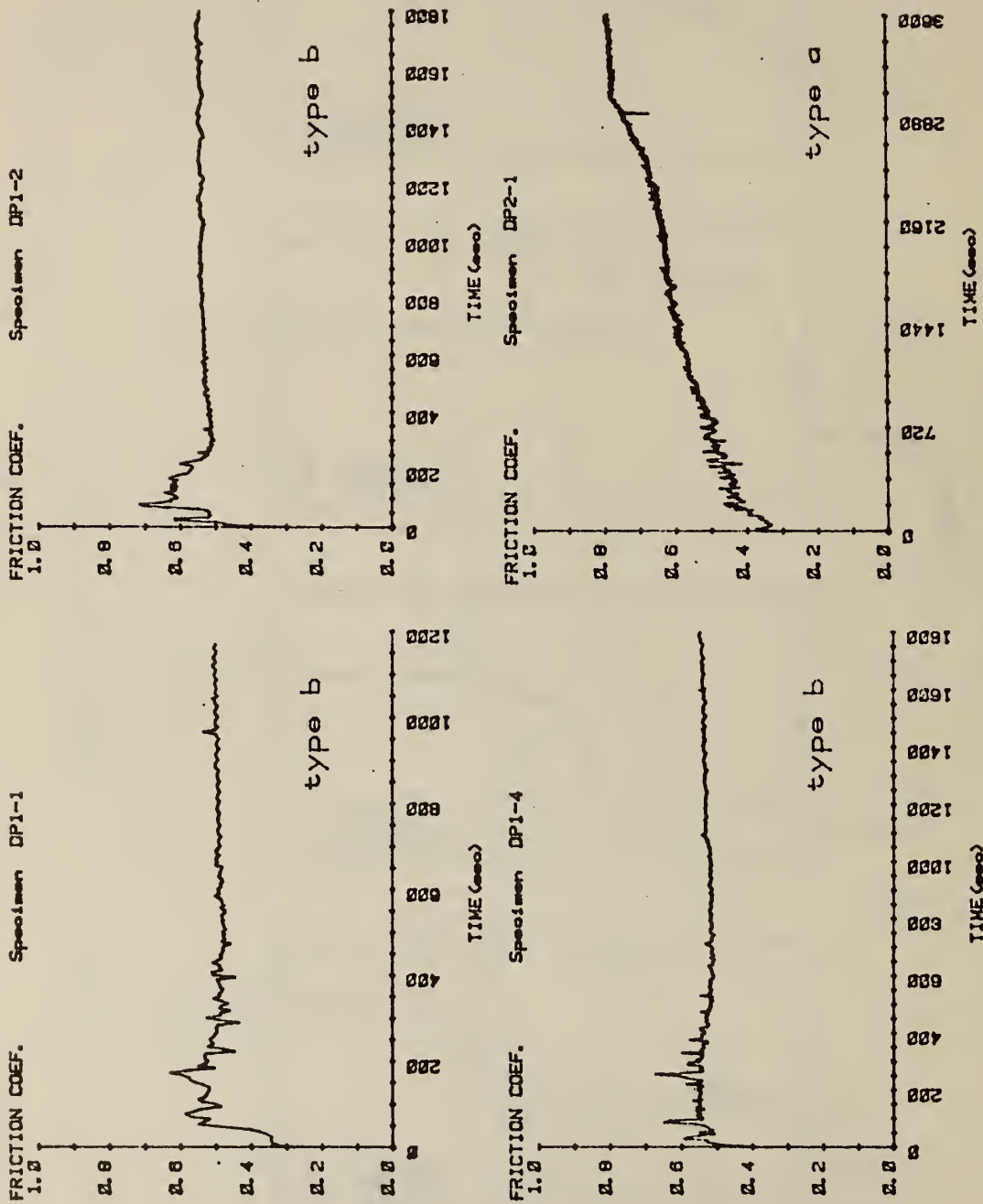


Fig. 9. (b) Comparison of friction curves for four DP80 steel specimens.

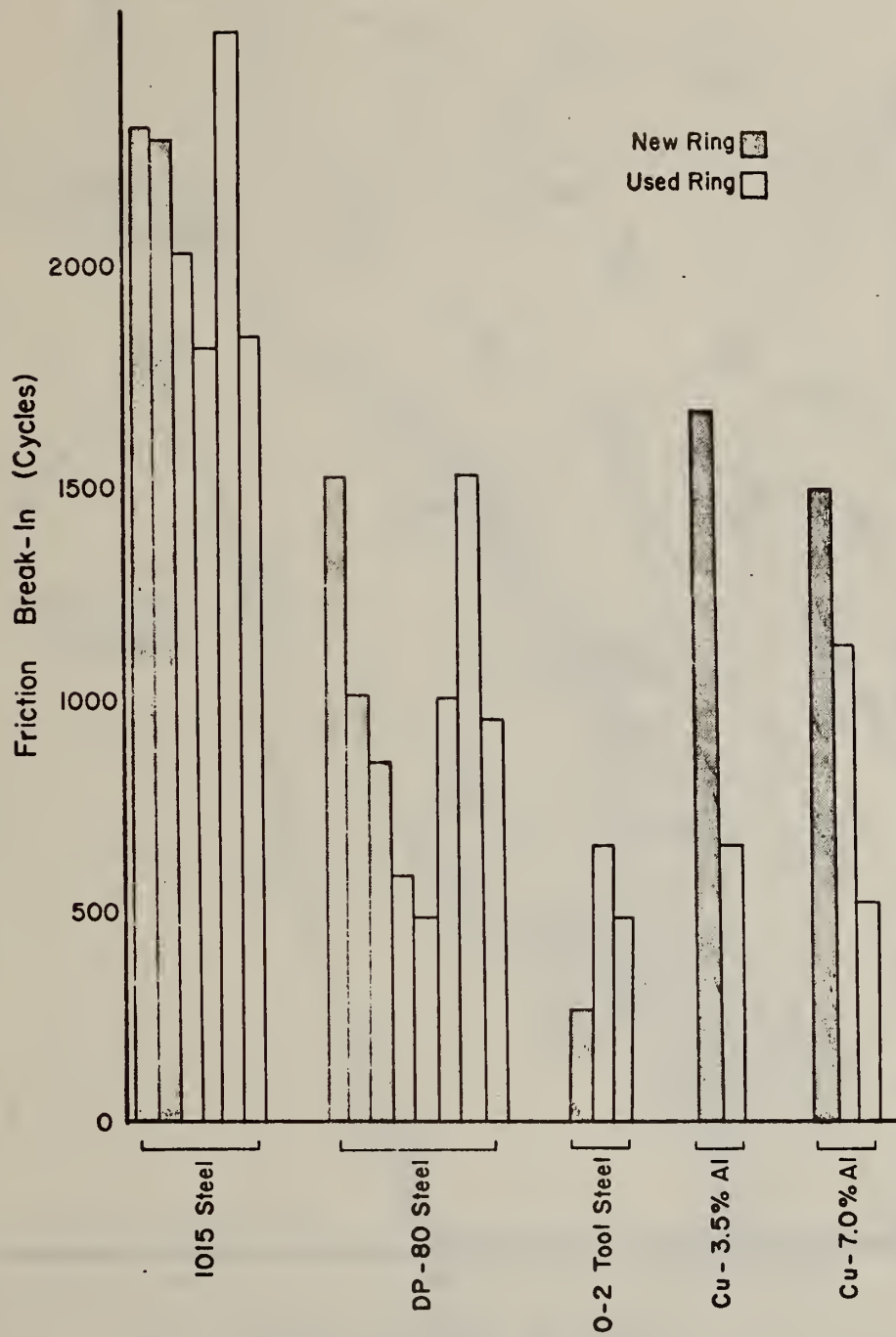


Fig. 10. Comparison of friction break-in characteristics for five alloys.

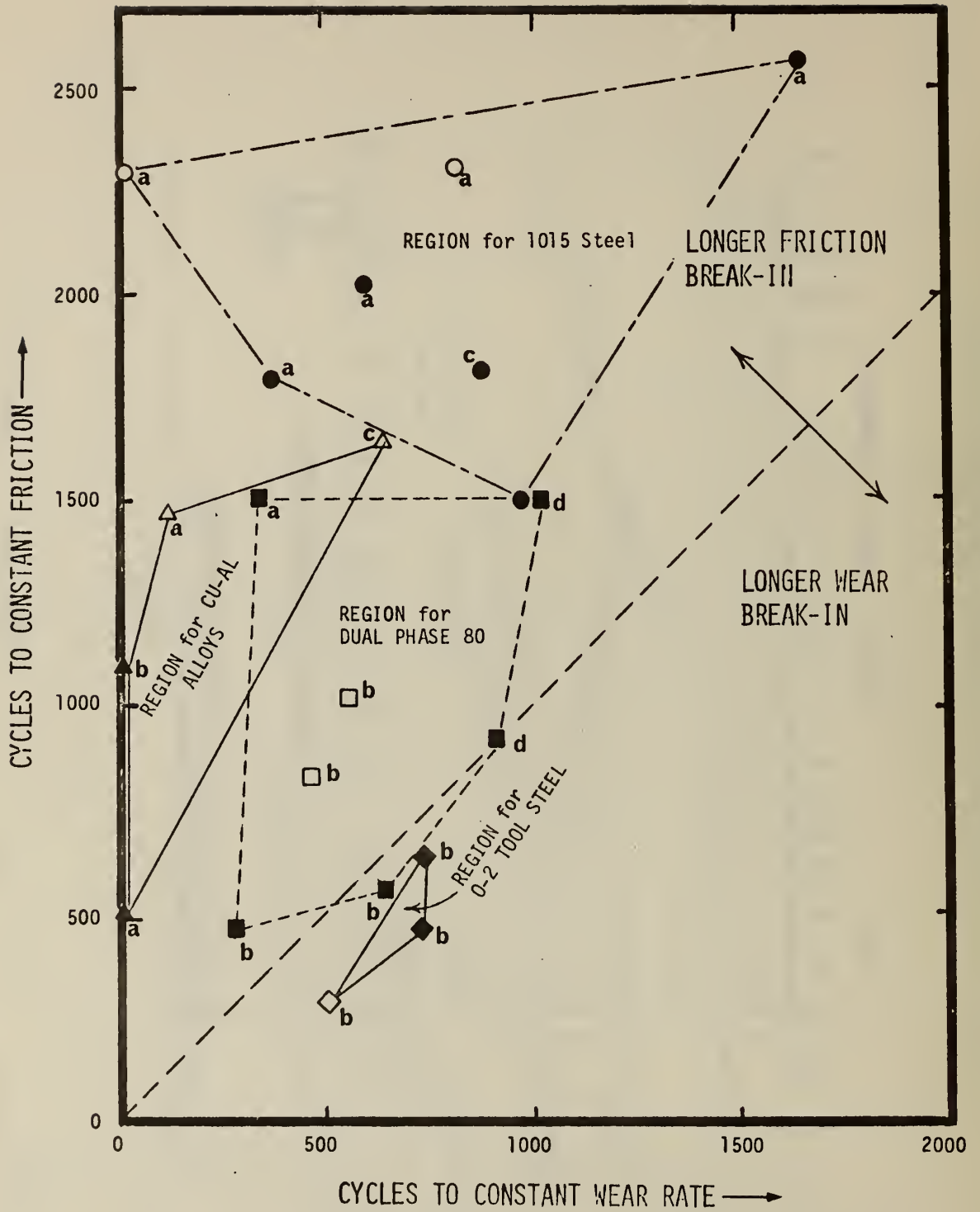


Fig. 11. Break-in map illustrating relationships between friction and wear break-in periods. Letters indicate break-in types from Fig. 9(a).



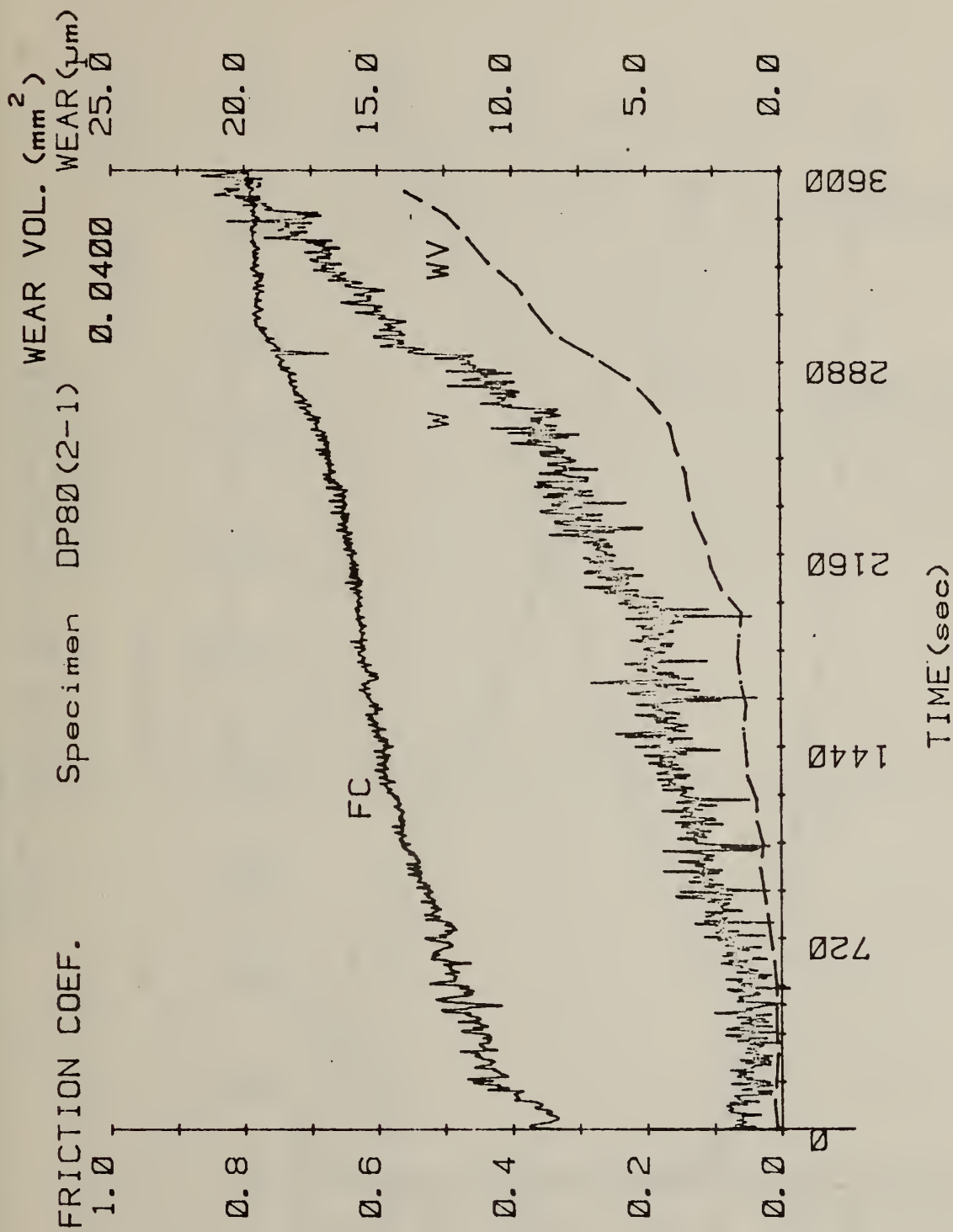


Fig. 12. Wear depth (W), wear volume (WV) and friction coefficient (FC) results for DP80 steel specimen.

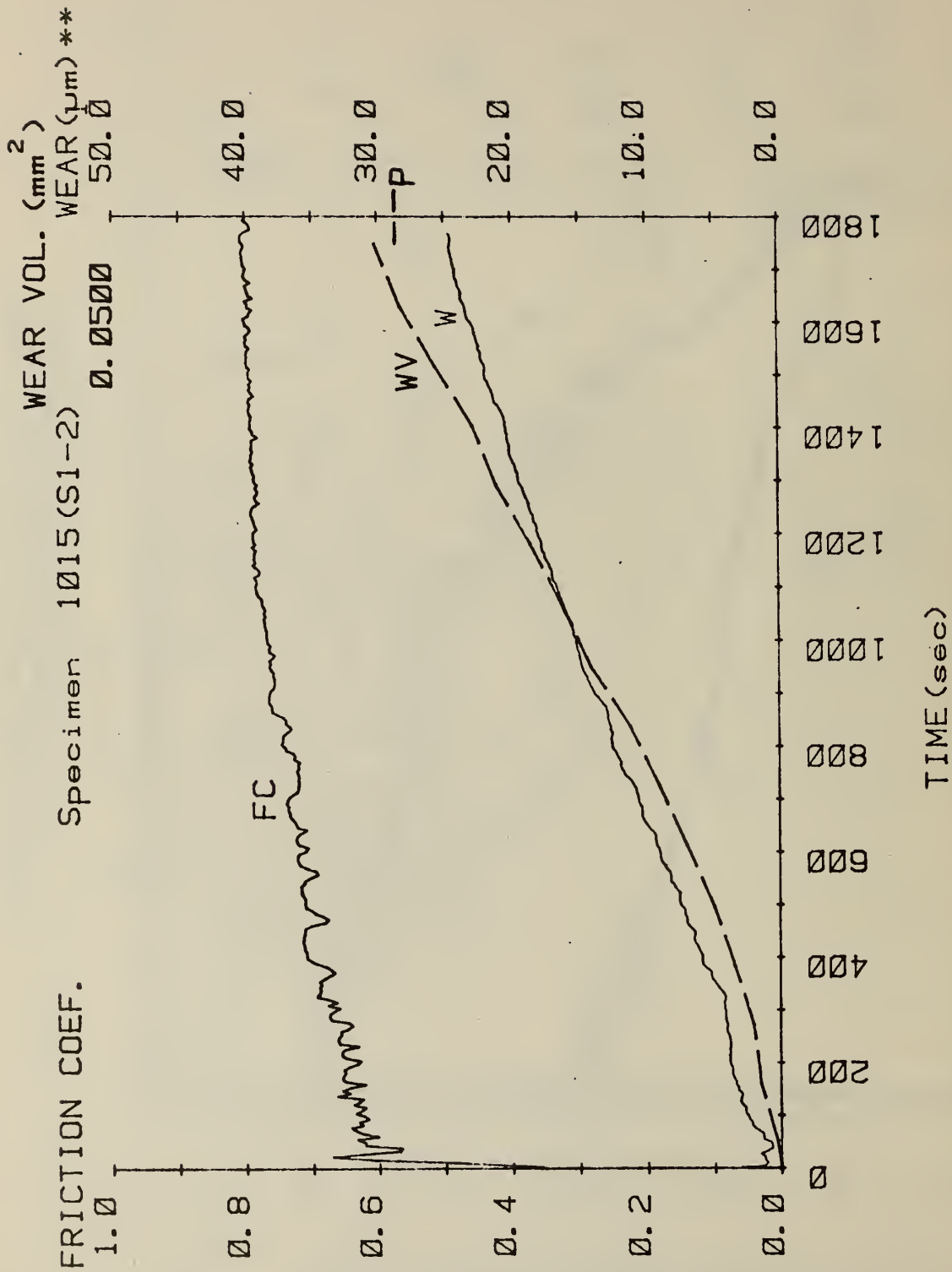


Fig. 13. (a) Wear depth (W), wear volume (WV) and friction coefficient (FC) results for 1015 steel specimen.

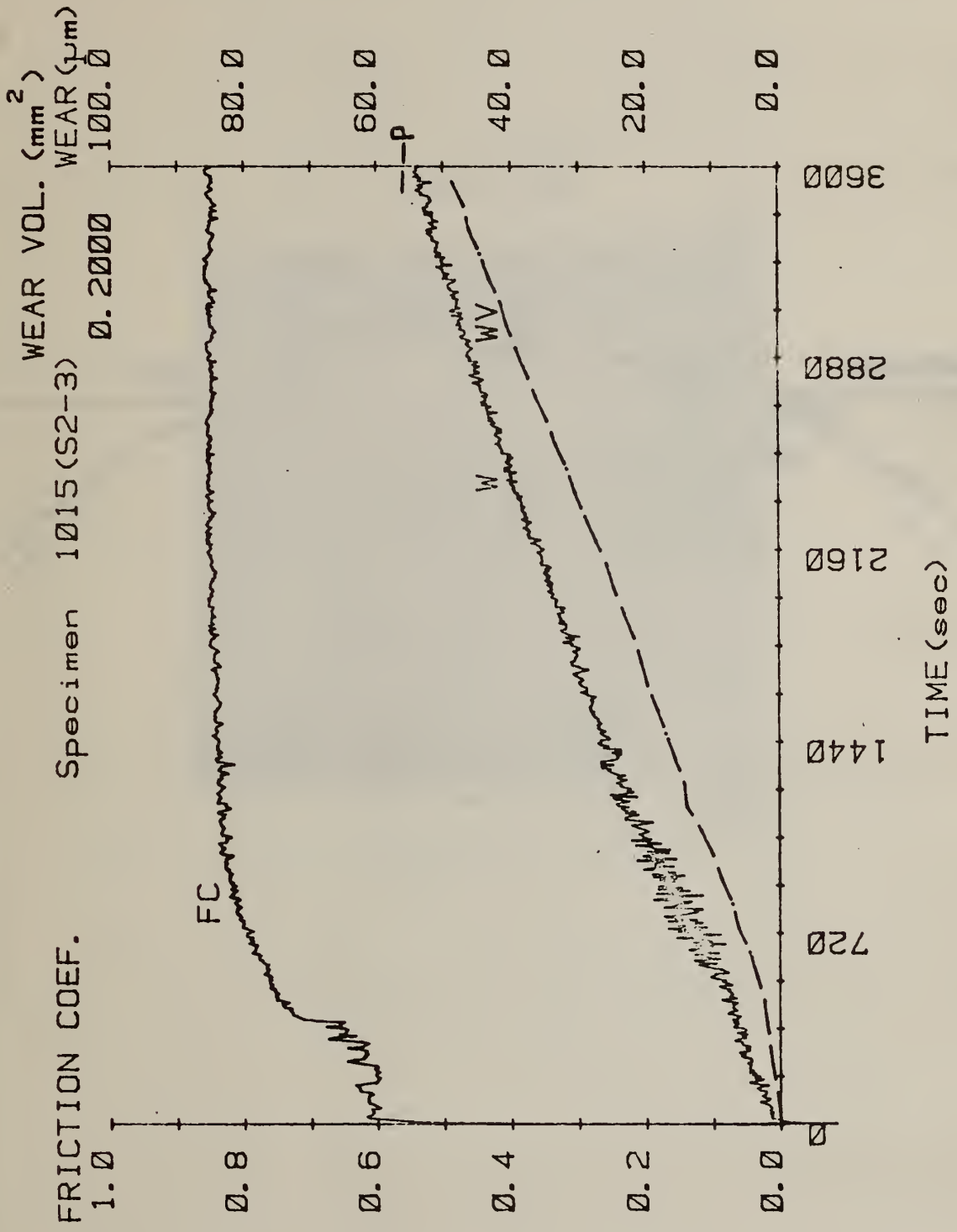


Fig. 13. (b) Wear depth (W), wear volume (WV) and friction coefficient (FC) results for 1015 steel specimen.

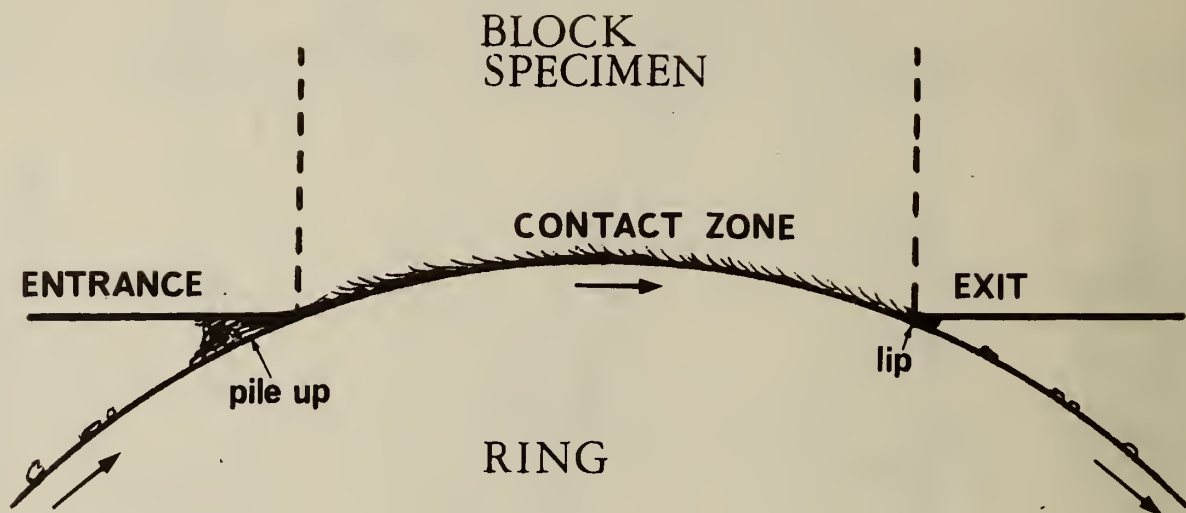


Fig. 14. Schematic representation of block-on-ring geometry.

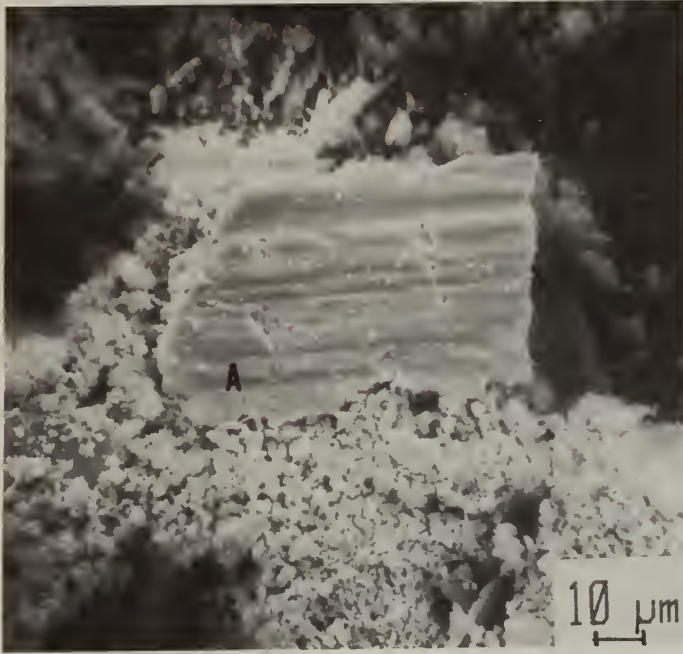


Fig. 15. Scanning electron micrograph of wear debris particles from 1015 steel specimen.

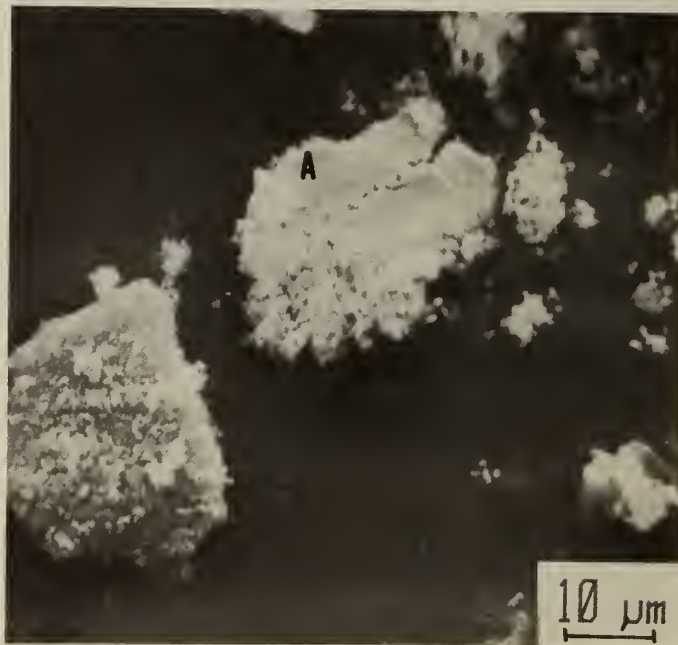
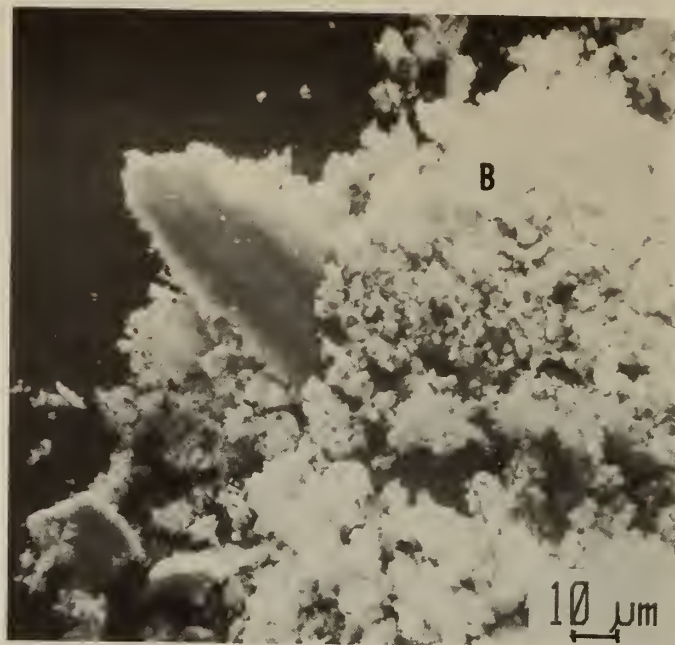


Fig. 16. Wear debris particles recovered from test of 1015 steel specimen. Note partial fracture of particles (A) in lower photograph. An aggregate of much smaller particles is seen at (B).

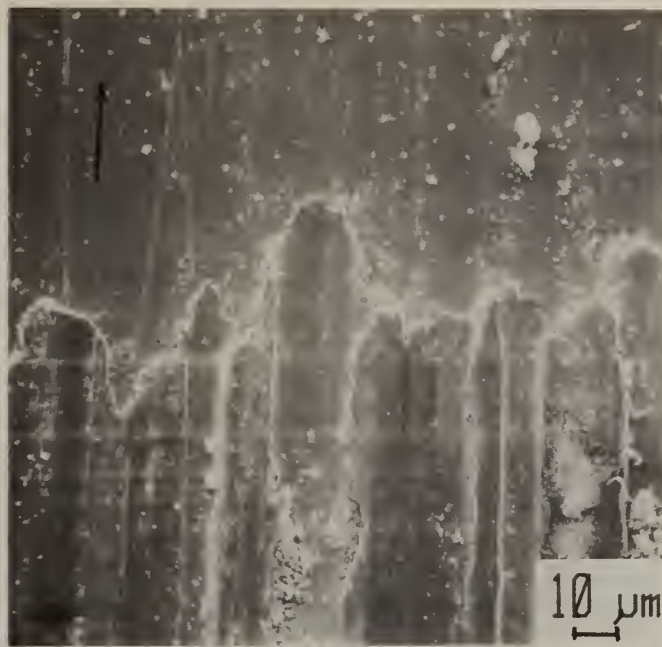


Fig. 17. Scanning electron micrograph of exit edge of wear scar on 1015 steel specimen surface. (a) arrow shows sliding direction. (b) evidence of deformation and fracture at edges of displaced material.

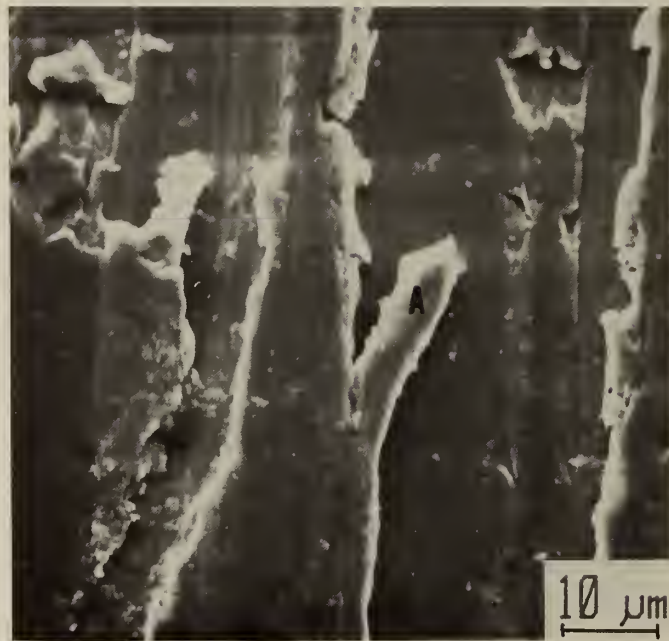


Fig. 18. Central region of wear scar on 1015 steel specimen. Wear particle formation appears underway at locations (A) where heavily deformed metal is present.



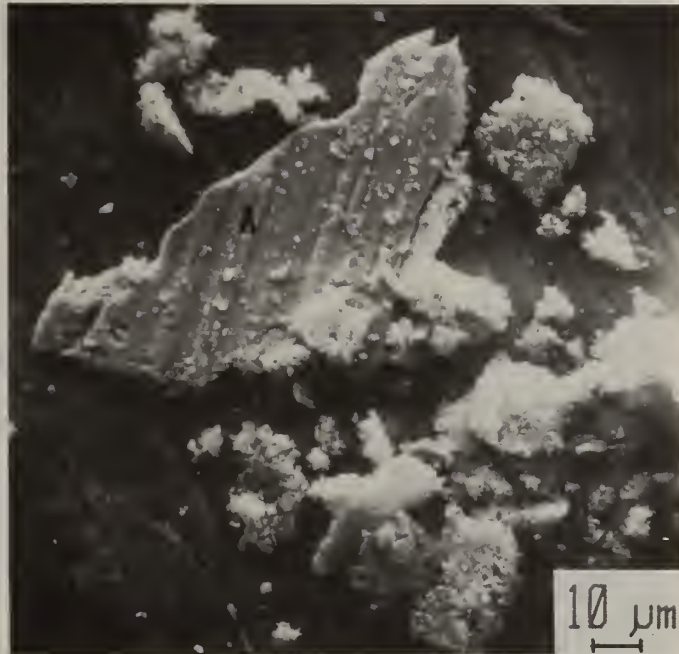


Fig. 19. Scanning electron micrograph of wear debris particles collected from test of DP80 steel specimen. Note scoring lines on surface of flat particle (A).

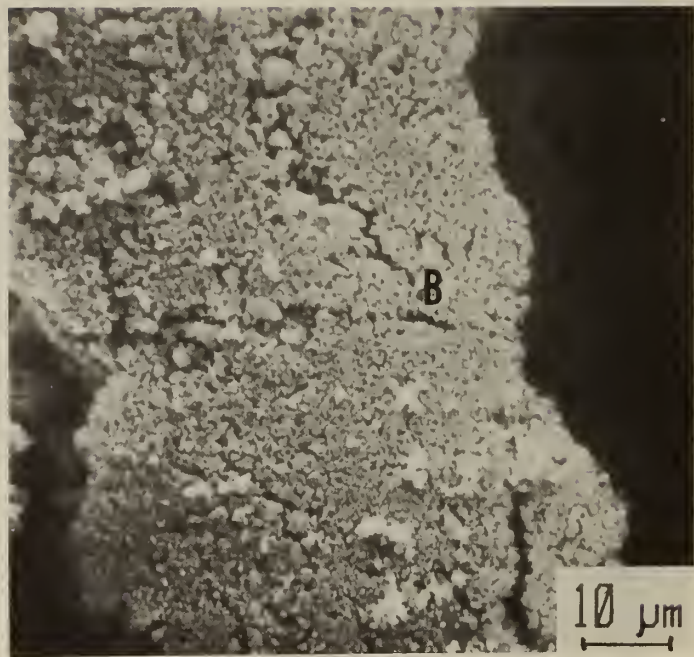
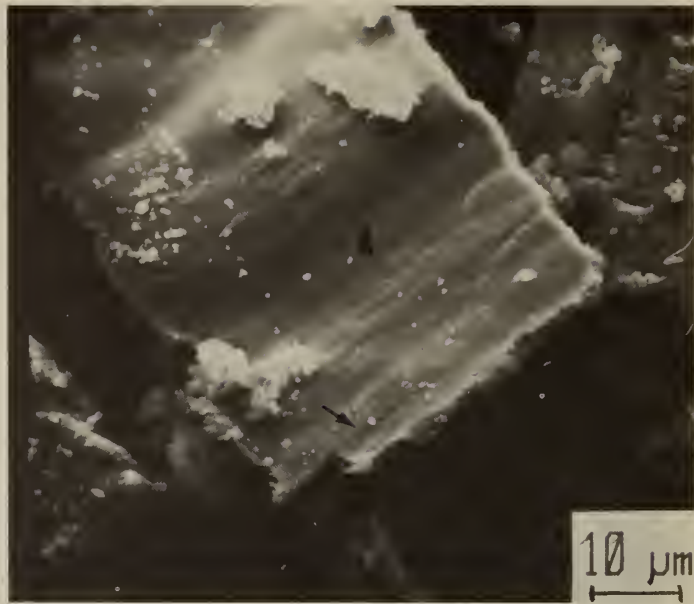


Fig. 20. Examples of large debris particles from DP80 wear tests having two different morphologies. Note crack-like feature in (A) at arrow.

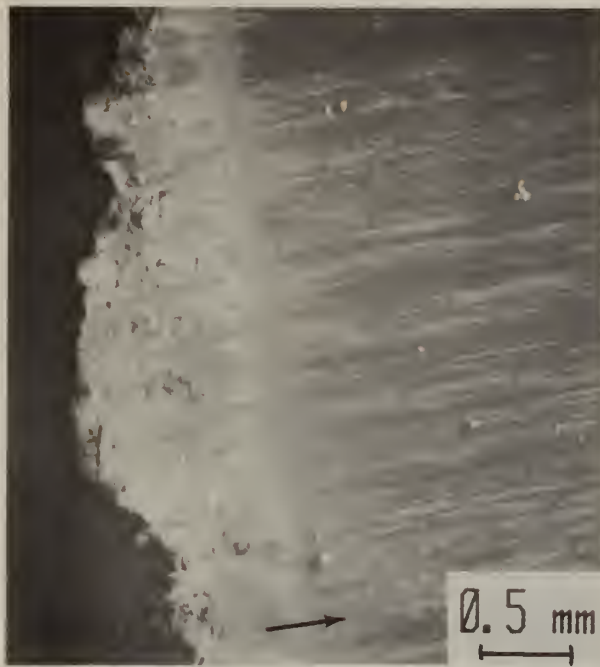


Fig. 21. (a) Entry region of wear scar on a DP80 specimen with sliding direction indicated by arrow.  
(b) Note crack in particle at (A) in one area of loose debris deposit.

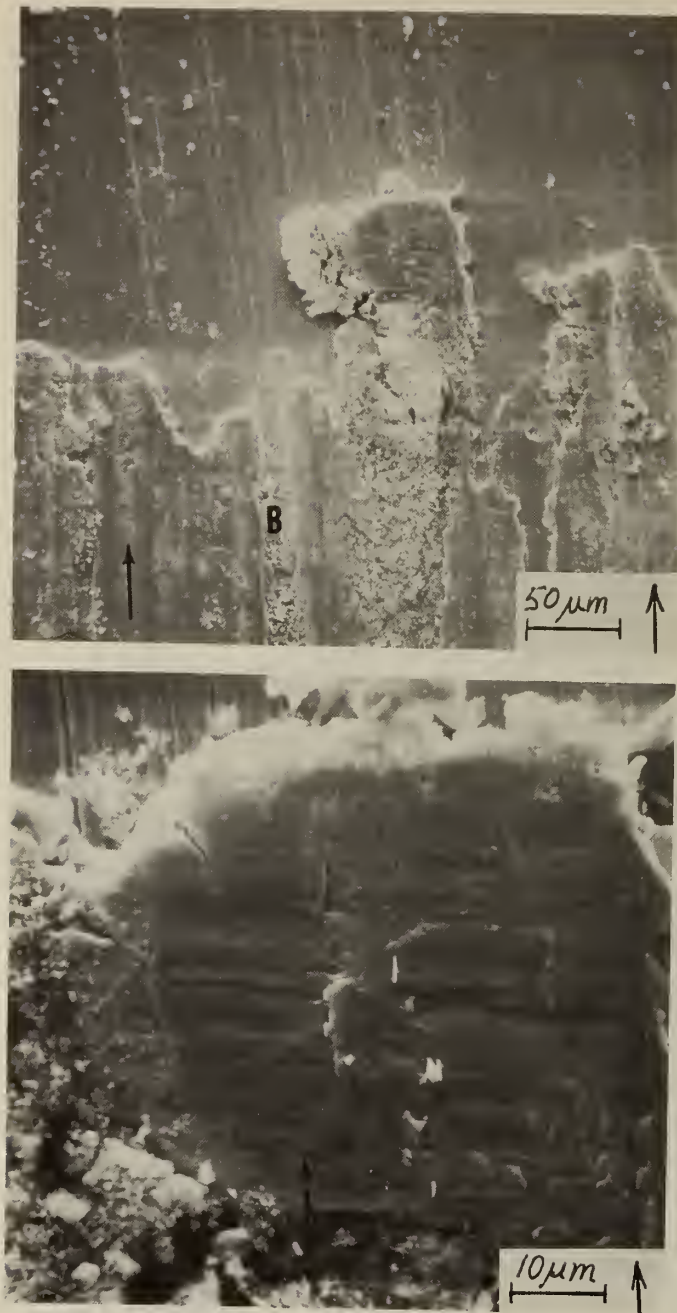


Fig. 22. (a) Scanning electron micrograph of exit edge of wear scar on a DP80 specimen. (b) Details of deformation markings and crack-like features. Arrow indicates sliding distance.

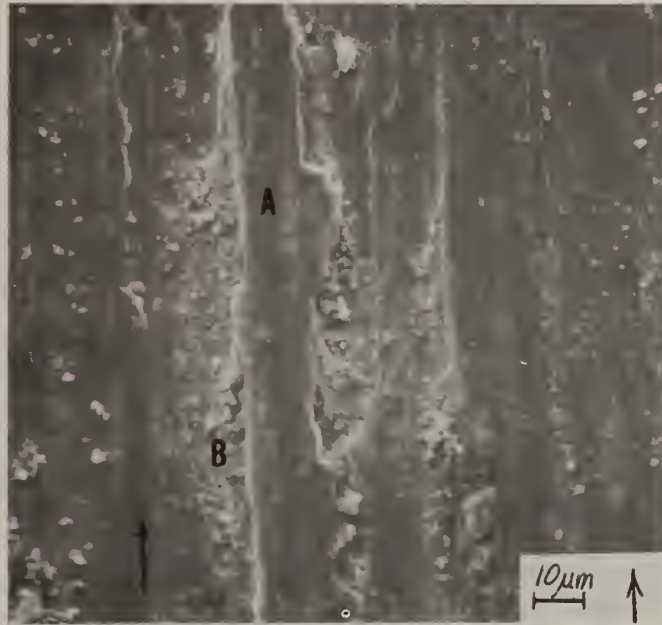


Fig. 23. Central region of wear scar on a DP80 specimen. Flat ridges of deformed metal (A) aligned in sliding direction (arrow) appear to carry imposed normal load.

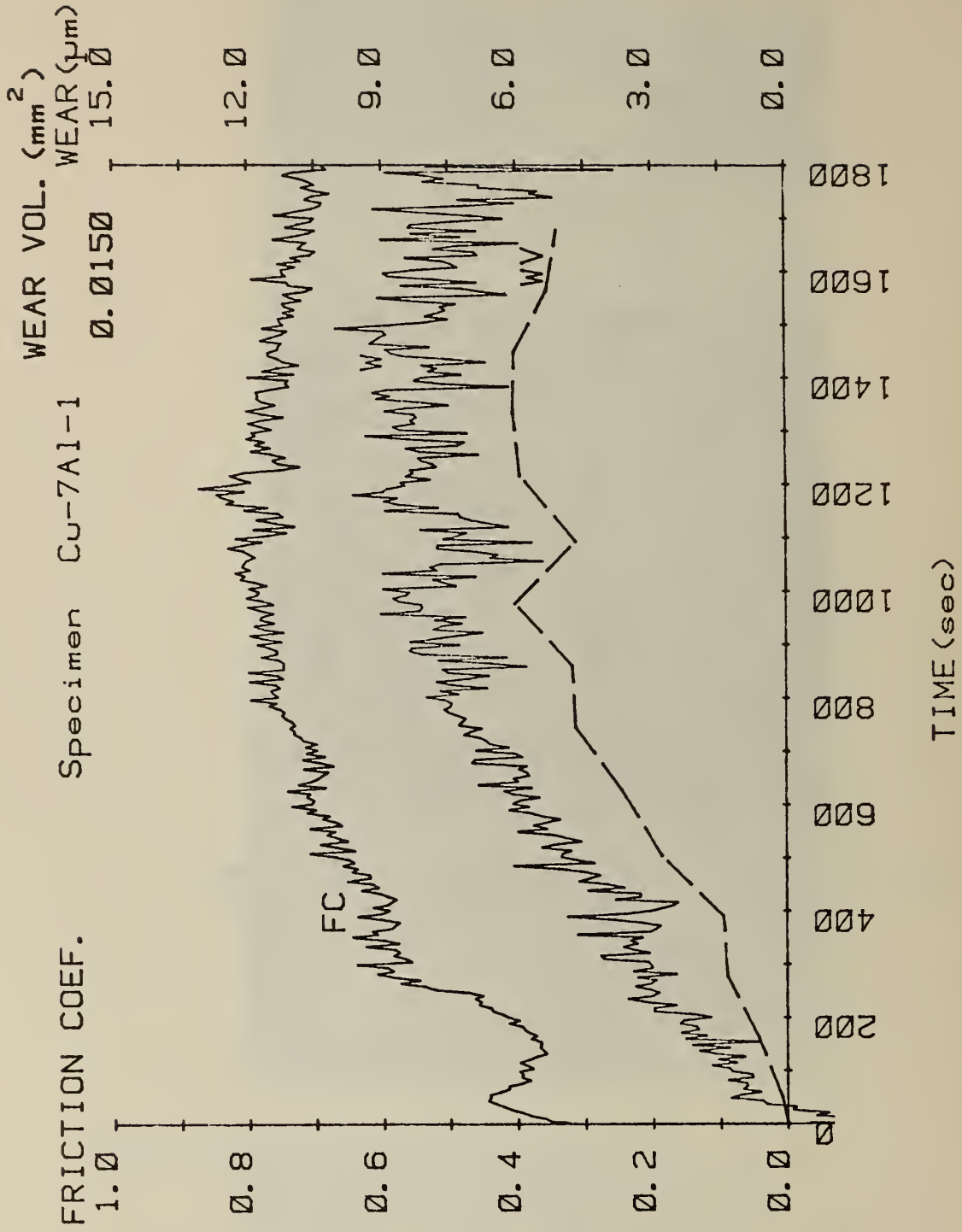


Fig. 24. Wear depth (W), wear volume (WV), and friction coefficient (FC) results for Cu-7.0Al specimen.

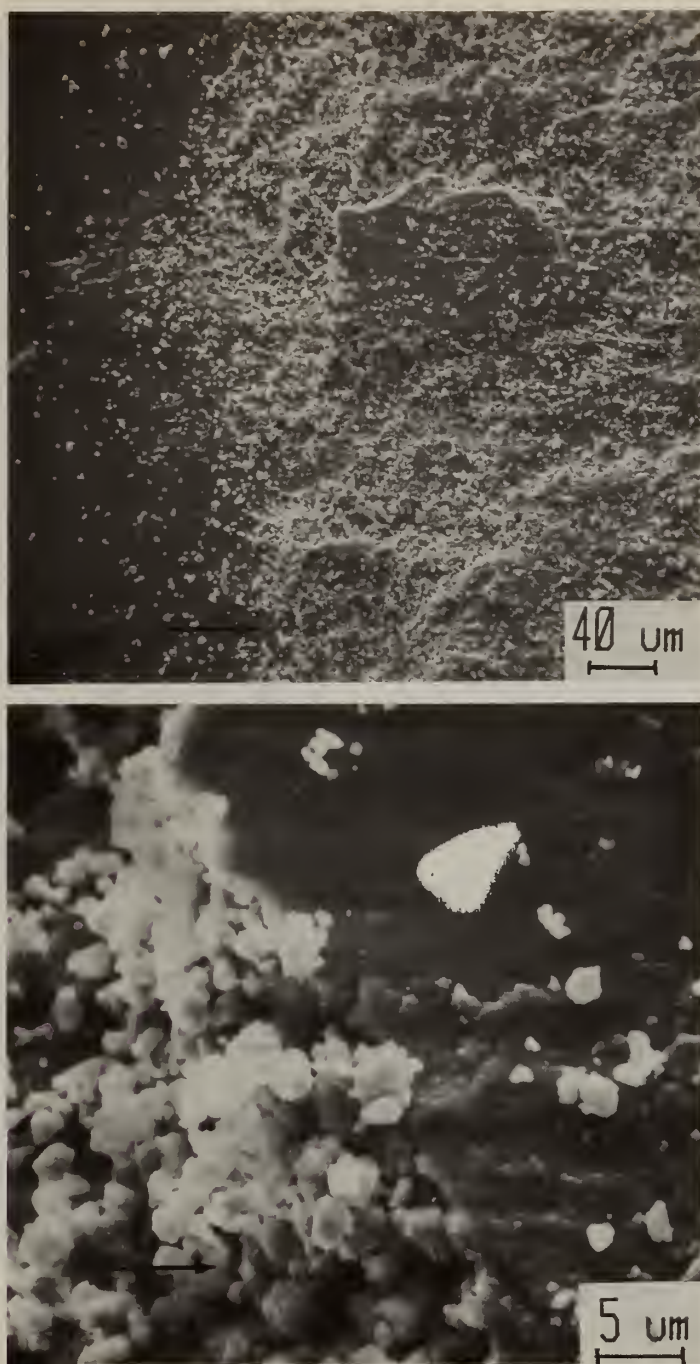


Fig. 25. Scanning electron micrograph of a large patch at the entrance edge of a wear scar on a Cu-7.0%Al specimen. Sliding direction is left to right (a) contact zone begins about one-third the distance from the right edge of the photomicrograph. (b) Higher magnification view of the leading edge of the patch. Small debris appears to be in the process of compaction, as indicated by the outlines on the patch surface at lower right.

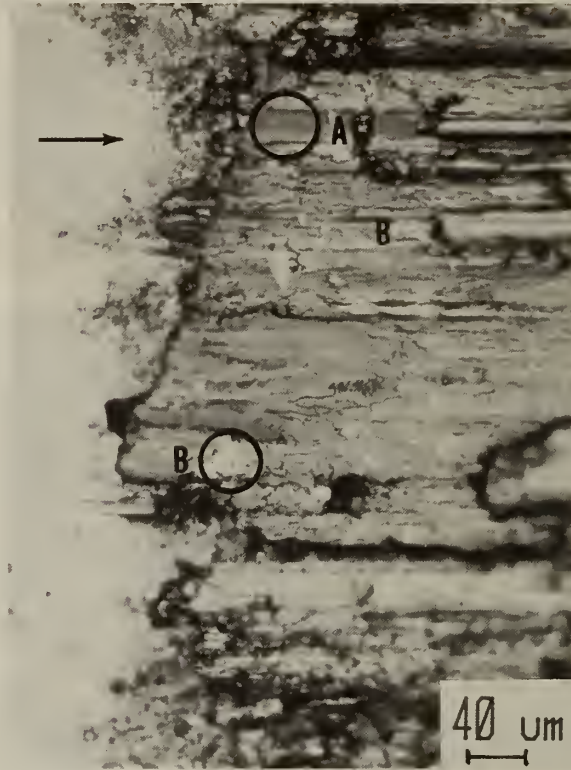


Fig. 26. Optical photomicrograph of an entrance edge patch on Cu-7.0Al showing gray (oxide) at A and light (metal) regions at B. Sliding direction is indicated by arrow.



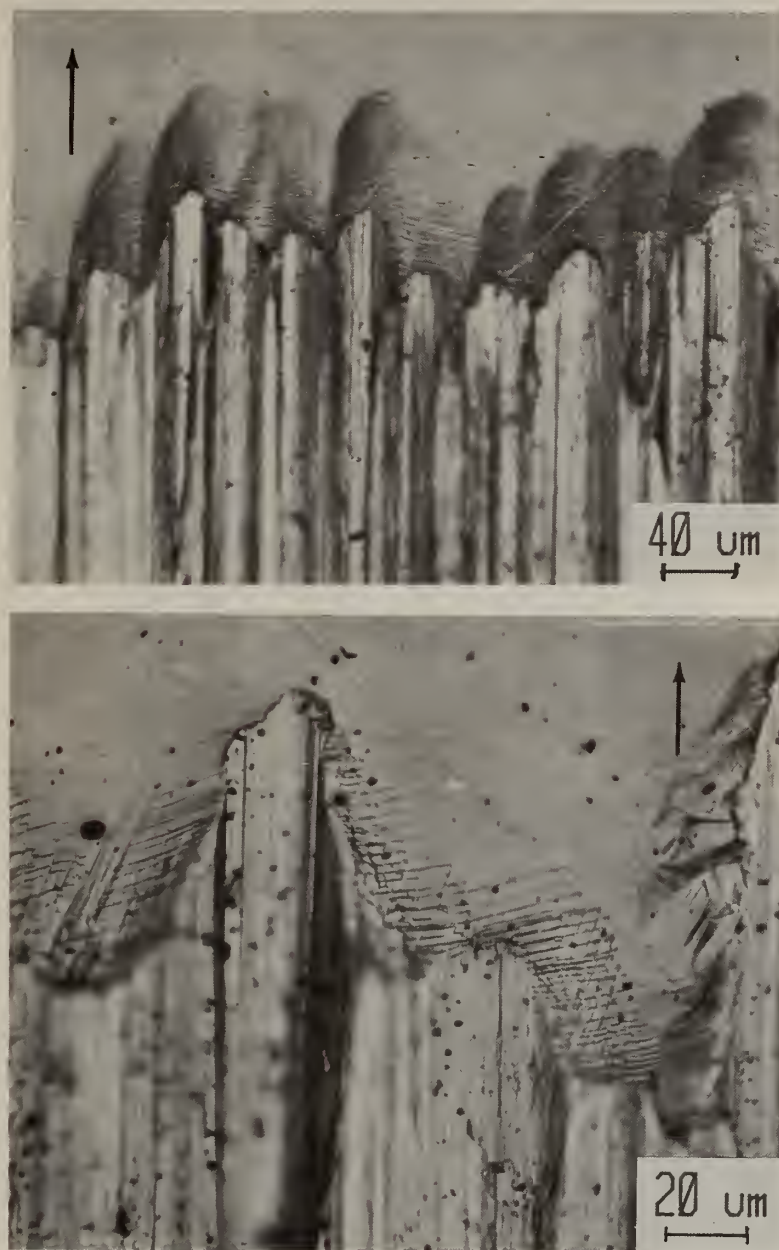


Fig. 27 Interference-contrast photomicrograph of the exit end of a Cu-7.0%Al block scar (a) surface topography reflects the deformation under the worn grooves (b) slip line fields at the exit end of the wear grooves. Sliding direction is given by arrows.

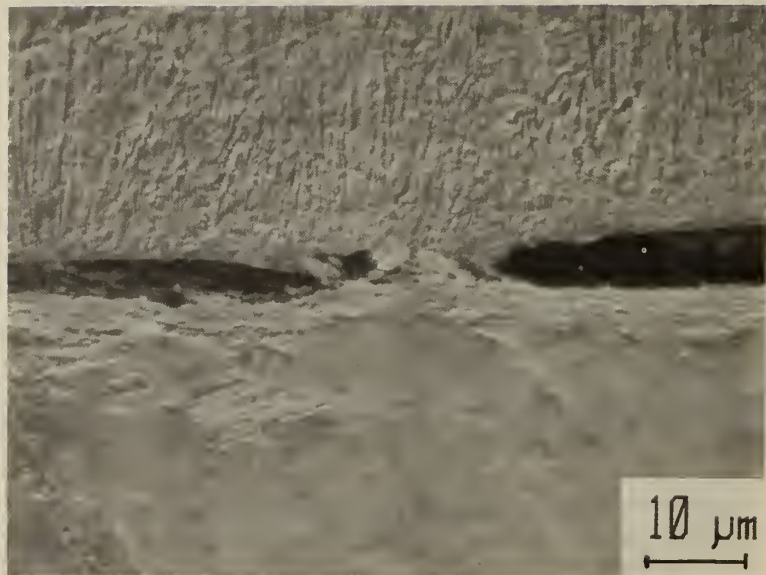
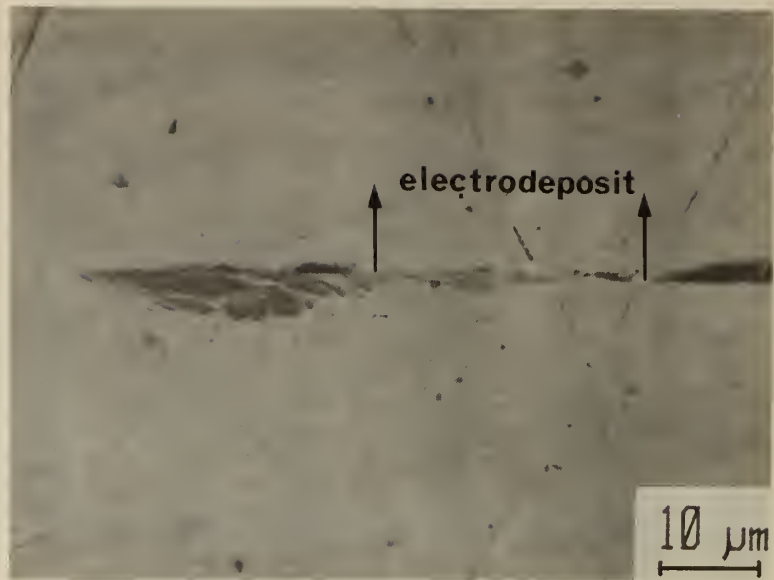


Fig. 28. (a) Cross section through Cu-7.0%Al block wear scar. Thickness of the lamellar zone is about 8  $\mu\text{m}$ . Unetched. (b) Lightly etched microstructure. Ring surface moved from right to left.

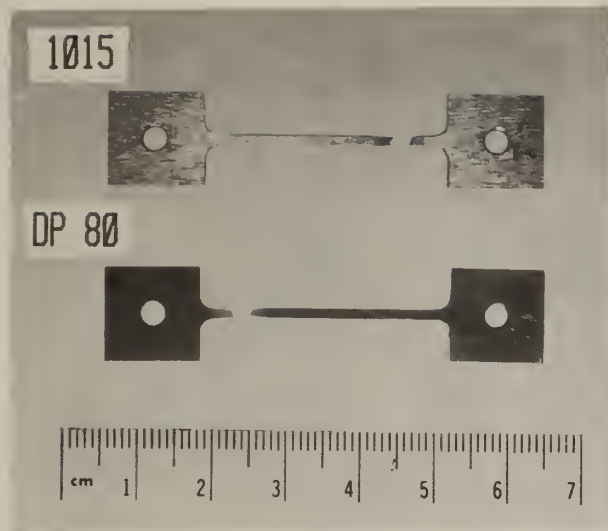


Fig. 29. Tensile specimen configurations.

Log True Stress

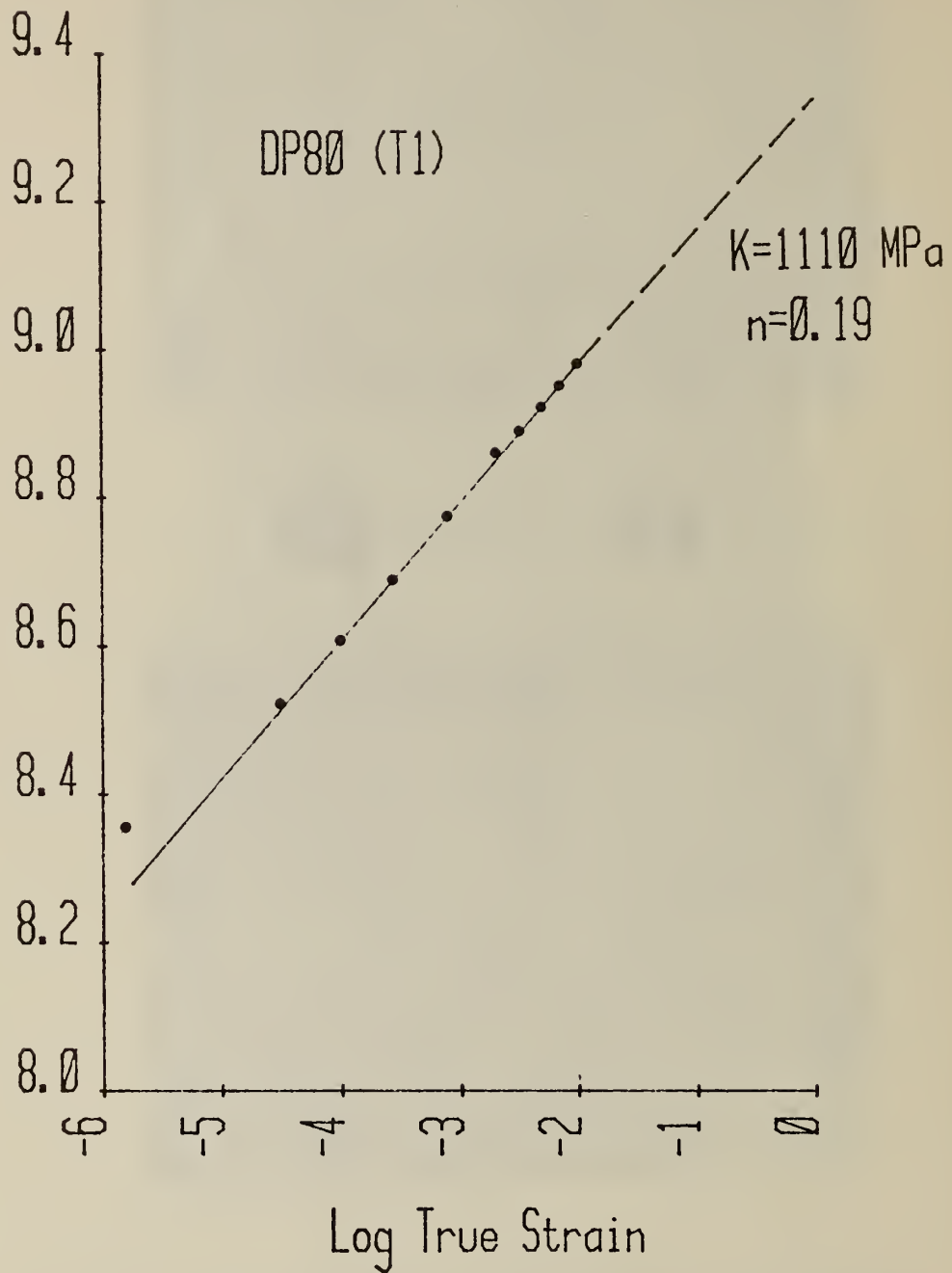


Fig. 30. Example of true stress-true strain results for one DP80 steel specimen.

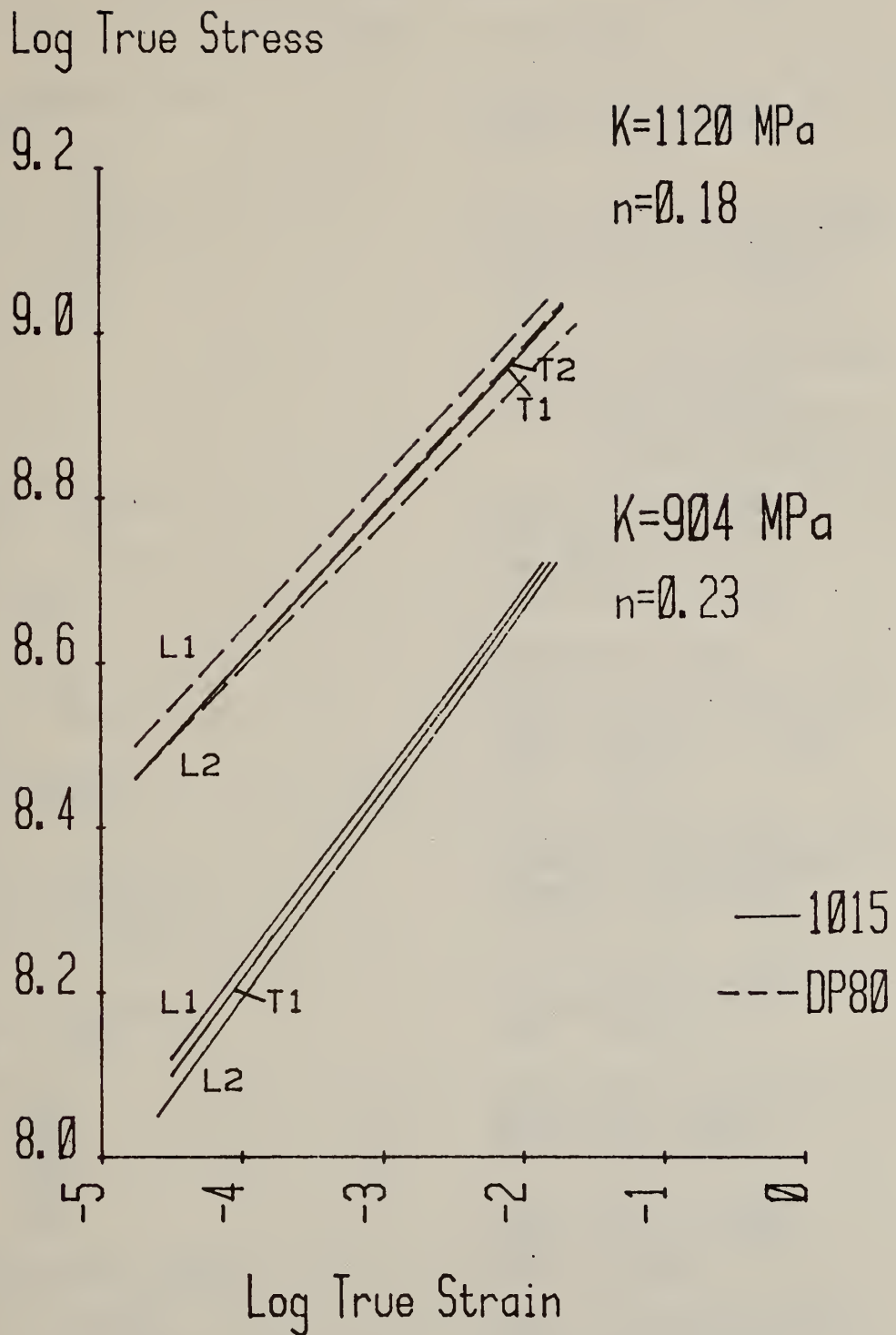


Fig. 31. Summary of uniaxial tensile deformation results on 1015 steel and DP80 steel specimens.



BASIC DISTRIBUTION LIST

Technical and Summary Reports

April 1978

<u>Organization</u>	<u>Copies</u>	<u>Organization</u>	<u>Copies</u>
Defense Documentation Center Cameron Station Alexandria, VA 22314	12	Naval Air Propulsion Test Center Trenton, NJ 08628 ATTN: Library	1
Office of Naval Research Department of the Navy 800 N. Quincy Street Arlington, VA 22217		Naval Construction Battalion Civil Engineering Laboratory Port Hueneme, CA 93043 ATTN: Materials Division	1
ATTN: Code 471	1	Naval Electronics Laboratory San Diego, CA 92152 ATTN: Electron Materials Sciences Division	1
Code 102	1		
Code 470	1		
Commanding Officer Office of Naval Research Branch Office Building 114, Section D 666 Summer Street Boston, MA 02210	1	Naval Missile Center Materials Consultant Code 3312-1 Point Mugu, CA 92041	1
Commanding Officer Office of Naval Research Branch Office 536 South Clark Street Chicago, IL 60605	1	Commanding Officer Naval Surface Weapons Center White Oak Laboratory Silver Spring, MD 20910 ATTN: Library	1
Office of Naval Research San Francisco Area Office One Hallidie Plaza Suite 601 San Francisco, CA 94102	1	David W. Taylor Naval Ship Research and Development Center Materials Department Annapolis, MD 21402	1
Naval Research Laboratory Washington, DC 20375		Naval Undersea Center San Diego, CA 92132 ATTN: Library	1
ATTN: Codes 6000	1	Naval Underwater System Center Newport, RI 02840 ATTN: Library	1
6100	1		
6300	1		
6400	1		
2627	1	Naval Weapons Center China Lake, CA 93555 ATTN: Library	1
Naval Air Development Center Code 302 Warminster, PA 18964 ATTN: Mr. F. S. Williams	1	Naval Postgraduate School Monterey, CA 93940 ATTN: Mechanical Engineering Department	1

BASIC DISTRIBUTION LIST (cont'd)

<u>Organization</u>	<u>Copies</u>	<u>Organization</u>	<u>Copies</u>
Naval Air Systems Command Washington, DC 20360 ATTN: Codes 52031 52032	1	NASA Headquarters Washington, DC 20546 ATTN: Code:RRM	1
Naval Sea System Command Washington, DC 20362 ATTN: Code 035	1	NASA Lewis Research Center 21000 Brookpark Road Cleveland, OH 44135 ATTN: Library	1
Naval Facilities Engineering Command Alexandria, VA 22331 ATTN: Code 03	1	National Bureau of Standards Washington, DC 20234 ATTN: Metallurgy Division Inorganic Materials Div.	1 1
Scientific Advisor Commandant of the Marine Corps Washington, DC 20380 ATTN: Code AX	1	Director Applied Physics Laboratory University of Washington 1013 Northeast Forthieth Street Seattle, WA 98105	1
Naval Ship Engineering Center Department of the Navy Washington, DC 20360 ATTN: Code 6101	1	Defense Metals and Ceramics Information Center Battelle Memorial Institute 505 King Avenue Columbus, OH 43201	1
Army Research Office P.O. Box 12211 Triangle Park, NC 27709 ATTN: Metallurgy & Ceramics Program	1	Metals and Ceramics Division Oak Ridge National Laboratory P.O. Box X Oak Ridge, TN 37380	1
Army Materials and Mechanics Research Center Watertown, MA 02172 ATTN: Research Programs Office	1	Los Alamos Scientific Laboratory P.O. Box 1663 Los Alamos, NM 87544 ATTN: Report Librarian	1
Air Force Office of Scientific Research Bldg. 410 Bolling Air Force Base Washington, DC 20332 ATTN: Chemical Science Directorate Electronics & Solid State Sciences Directorate	1 1	Argonne National Laboratory Metallurgy Division P.O. Box 229 Lemont, IL 60439	1 1
Air Force Materials Laboratory Wright-Patterson AFB Dayton, OH 45433	1	Brookhaven National Laboratory Technical Information Division Upton, Long Island New York 11973 ATTN: Research Library	1
Library Building 50, Rm 134 Lawrence Radiation Laboratory Berkeley, CA	1	Office of Naval Research Branch Office 1030 East Green Street Pasadena, CA 91106	1



REPORT DOCUMENTATION PAGE		READ INSTRUCTIONS BEFORE COMPLETING FORM	
1. REPORT NUMBER NBSIR 80- 2058 (ONR)	2. GOVT ACCESSION NO.	3. RECIPIENT'S CATALOG NUMBER	
4. TITLE (and Subtitle) STUDIES OF MICROSCOPIC ASPECTS OF WEAR PROCESSES IN METALS		5. TYPE OF REPORT & PERIOD COVERED Annual Report Jan. 1979 - Dec. 1979	
		6. PERFORMING ORG. REPORT NUMBER	
7. AUTHOR(s) A. W. Ruff P. J. Blau		8. CONTRACT OR GRANT NUMBER(s)  N00014-79-F-0034	
9. PERFORMING ORGANIZATION NAME AND ADDRESS  National Bureau of Standards Washington, DC		10. PROGRAM ELEMENT, PROJECT, TASK AREA & WORK UNIT NUMBERS	
11. CONTROLLING OFFICE NAME AND ADDRESS Dept. of Navy Office of Naval Research - ATTN: R. Burton Arlington, VA 22217		12. REPORT DATE March 1980	
		13. NUMBER OF PAGES 34	
14. MONITORING AGENCY NAME & ADDRESS (if different from Controlling Office)		15. SECURITY CLASS. (of this report)  Unclassified	
		15a. DECLASSIFICATION/DOWNGRADING SCHEDULE	
16. DISTRIBUTION STATEMENT (of this Report)			
17. DISTRIBUTION STATEMENT (of the abstract entered in Block 20, if different from Report)  Unlimited			
18. SUPPLEMENTARY NOTES			
19. KEY WORDS (Continue on reverse side if necessary and identify by block number)  Copper; electron microscopy; friction; metals; plastic deformation; steel; surfaces; wear; wear debris			
20. ABSTRACT (Continue on reverse side if necessary and identify by block number)  Wear experiments have been conducted in copper alloys and steel under dry sliding conditions in order to study the microscopic aspects of wear and the mechanisms involved. Two experimental wear test systems have been developed: a linear sliding tester and a block-on-ring computer controlled tester. Preliminary findings have compared the wear rates of three different steels, one a high strength-low alloy "dual phase"			

20. Abstract (continued)

steel, and two copper-aluminum alloys. Worn surface and subsurface morphologies have been studied using optical and scanning electron microscopy. Wear debris particles have been recovered from the tests and compared in morphological characteristics between the materials. Mechanical properties measurements of two of the steels were carried out to determine strain hardening characteristics for comparison with wear behavior. Micro-hardness measurements have also been made. Initial wear rate and friction transients for tests in laboratory air and argon have been examined to study processes involved in the early stages of sliding.

U.S. DEPT. OF COMM. BIBLIOGRAPHIC DATA SHEET	1. PUBLICATION OR REPORT NO.  NBSIR 80-2058 (ONR)	2. Gov't. Accession No.	3. Recipient's Accession No.
4. TITLE AND SUBTITLE  Studies of Microscopic Aspects of Wear Processes in Metals		5. Publication Date  June 1980	
		6. Performing Organization Code	
7. AUTHOR(S)  A. W. Ruff and P. J. Blau		8. Performing Organ. Report No.	
9. PERFORMING ORGANIZATION NAME AND ADDRESS  NATIONAL BUREAU OF STANDARDS DEPARTMENT OF COMMERCE WASHINGTON, DC 20234		10. Project/Task/Work Unit No.	
		11. Contract/Grant No.  N00014-79-F-0034	
12. SPONSORING ORGANIZATION NAME AND COMPLETE ADDRESS (Street, City, State, ZIP)  Office of Naval Research Department of the Navy Arlington, VA 22217		13. Type of Report & Period Covered  Annual	
		14. Sponsoring Agency Code	
15. SUPPLEMENTARY NOTES  <input type="checkbox"/> Document describes a computer program; SF-185, FIPS Software Summary, is attached.			
16. ABSTRACT (A 200-word or less factual summary of most significant information. If document includes a significant bibliography or literature survey, mention it here.)  Wear experiments have been conducted in copper alloys and steels under dry sliding conditions in order to study the microscopic aspects of wear and the mechanisms involved. Two experimental wear test systems have been developed: a linear sliding tester and a block-on-ring computer controlled tester. Preliminary findings have compared the wear rates of three different steels, one a high strength-low alloy "dual phase" steel, and two copper-aluminum alloys. Worn surface and subsurface morphologies have been studied using optical and scanning electron microscopy. Wear debris particles have been recovered from the tests and compared in morphological characteristics between the materials. Mechanical properties measurements of two of the steels were carried out to determine strain hardening characteristics for comparison with wear behavior. Micro-hardness measurements have also been made. Initial wear rate and friction transients for tests in laboratory air and argon have been examined to study processes involved in the early stages of sliding.			
17. KEY WORDS (six to twelve entries; alphabetical order; capitalize only the first letter of the first key word unless a proper name; separated by semicolons)  Copper; electron microscopy; friction; metals; plastic deformation; steel; surfaces; wear; wear debris.			
18. AVAILABILITY  <input checked="" type="checkbox"/> Unlimited  <input type="checkbox"/> For Official Distribution. Do Not Release to NTIS  <input type="checkbox"/> Order From Sup. of Doc., U.S. Government Printing Office, Washington, DC 20402, SD Stock No. SN003-003-  <input checked="" type="checkbox"/> Order From National Technical Information Service (NTIS), Springfield, VA. 22161		19. SECURITY CLASS (THIS REPORT)  UNCLASSIFIED	21. NO. OF PRINTED PAGES  72
		20. SECURITY CLASS (THIS PAGE)  UNCLASSIFIED	22. Price  \$7.00

